A disease-associated gene desert orchestrates macrophage inflammatory responses via ETS2

Authors:

Stankey CT[1,2]*, Bourges C[1]*, Turner-Stokes T[1,2], Piedade AP[1], Palmer-Jones C[3], Papa I[1], Dos Silva dos Santos M[4], Randzavola LO[2], Speidel L[5,6], Parkes EC[1], Edwards W[7], Rochford AP[3], Murray CD[3], MacRae JI[4], Skoglund P[5], Wallace C[7,9], Cader MZ[7,8], Thomas DC[2], Lee JC[1,3].

Affiliations:

[1] Genetic Mechanisms of Disease Laboratory, The Francis Crick Institute, London, UK

[2] Department of Immunology and Inflammation, Imperial College London, UK

[3] Department of Gastroenterology, UCL Institute of Liver and Digestive Diseases, Royal Free Hospital, Pond St, London, UK

[4] Metabolomics STP, The Francis Crick Institute, London, UK

[5] Ancient Genomics Laboratory, The Francis Crick Institute, London, UK

[6] Genetics Institute, University College London, UK

[7] Cambridge Institute of Therapeutic Immunology and Infectious Disease, Jeffrey Cheah Biomedical Centre, University of Cambridge, Cambridge, UK

[8] Department of Medicine, University of Cambridge, Addenbrooke's Hospital, Cambridge, UK

[9] MRC Biostatistics Unit, Cambridge Institute of Public Health, Cambridge, UK

* These authors contributed equally to this work

Correspondence: james.lee@crick.ac.uk

Abstract

Increasing global rates of autoimmune and inflammatory disease present a burgeoning threat to human health[1]. This is compounded by the limited efficacy of available treatments[1] and high failure rates during drug development[2] – underscoring an urgent need to better understand disease mechanisms. Here we show how genetics could address this challenge. By investigating an intergenic haplotype on chr21q22, independently linked to inflammatory bowel disease (IBD), ankylosing spondylitis, primary sclerosing cholangitis and Takayasu's arteritis[3-6], we discover that the causal gene, *ETS2*, is a master regulator of inflammatory responses in human macrophages and delineate how the risk haplotype increases *ETS2* expression. Genes regulated by ETS2 were prominently expressed in affected tissues from chr21q22-associated diseases and more enriched for IBD GWAS hits than almost all previously described pathways. Overexpressing *ETS2* in resting macrophages produced an activated effector state that phenocopied intestinal macrophages from IBD[7], with upregulation of multiple drug targets including TNFα and IL-23. Using a database of cellular signatures[8], we identify drugs that could modulate this pathway and validate the potent anti-inflammatory activity of one class of small molecules *in vitro* and *ex vivo*. Together, this highlights the potential for common genetic associations to improve both the understanding and treatment of human disease.

Currently, nearly 5% of the world's population are affected by at least one autoimmune or inflammatory disease. These heterogeneous conditions, which range from Crohn's disease and ulcerative colitis (collectively IBD) to psoriasis and rheumatoid arthritis, share a common need for better treatments, but only ~10% of drugs entering clinical development ever become approved therapies[2]. This high failure rate is principally due to a lack of efficacy[9] or – put another way – because the pathways being targeted are less important than they were assumed to be. Genetics provides a unique opportunity to elucidate disease mechanisms, with hundreds of regions of the human genome now directly linked to the pathogenesis of one or more autoimmune or inflammatory disease[10]. Indeed, drugs that target pathways implicated by genetics have a substantially higher chance of becoming approved therapies[11].

To fully realise the potential of genetics, however, knowledge of where risk variants lie must first be translated into an understanding of how they contribute to disease[10]. This is a formidable challenge since most disease-associated genetic variants do not lie in coding DNA, where effects on protein sequence/structure can be easily predicted, but in the enigmatic non-coding genome where the same DNA sequence can have different biological functions depending on the cell-type and/or external stimuli[10]. Most risk variants are thought to affect gene regulation[12], but the need to identify the causal gene(s) – which may lie up to one million bases away – and the causal cell-type(s), which may only express the causal gene under specific conditions, have hindered attempts to discover disease mechanisms. For example, although genome-wide association studies (GWAS) have identified over 240 IBD risk loci[3], fewer than 10 have been mechanistically resolved and, to date, none have led to new therapies.

Molecular mechanisms at the pleiotropic chr21q22 locus

Several genetic variants predispose to more than one disease – highlighting both their biological importance and an opportunity to discover shared disease mechanisms. One

notable example is an intergenic region on chr21q22, where the major (risk) allele haplotype has been independently associated with five different inflammatory diseases[3-6]. Although the associated locus does not contain any genes, there are several nearby candidates including *PSMG1*, *BRWD1* and *ETS2* (**Fig.1a**), all of which have been proposed to be potentially causal in previous studies[3-6,13]. The underlying biological mechanisms, however, remain unknown. We hypothesised that this intergenic locus must contain a distal enhancer and – since the associated diseases are all immune-mediated despite affecting different organs – searched for evidence of enhancer activity in disease-relevant immune cell-types. Using H3K27ac ChIP-seq data, which marks active enhancers/promoters, we found that this locus contains a monocyte/macrophage-specific enhancer (**Fig.1a**). Monocytes and monocyte-derived macrophages play a central role in the pathogenesis of many autoimmune and inflammatory diseases, producing cytokines that are often targeted by the most effective therapies[14].

To identify the gene regulated by this enhancer, we first considered publicly-available data from human monocytes, including promoter-capture Hi-C[15] and eQTL datasets[16]. We found that the disease-associated locus physically interacts with the promoter of *ETS2*, the most distant of the candidate genes (located 290-kb away) and that the risk haplotype correlates with higher *ETS2* expression, especially after monocyte activation (**Extended Data Fig.1**). Interestingly, however, the disease association was predicted to share a causal variant not with the strong eQTL in activated monocytes, but rather with a weaker eQTL in resting monocytes (**Extended Data Fig.1**). To directly confirm the identity of the target gene, we deleted the 1.85-kb enhancer region in primary human monocytes using CRISPR-Cas9 ribonucleoprotein (RNP) complexes containing gRNAs that flank the enhancer (**Fig.1b**, **Extended Data Fig.2**). These cells were then cultured with combination of inflammatory mediators, including TNFα (a pro-inflammatory cytokine), prostaglandin E2 (a pro-inflammatory lipid) and Pam3CSK4 (a TLR1/2 agonist). This model, termed "TPP", was designed to mimic a chronic inflammatory environment[17], and better recapitulates the state

4

of patient-derived monocytes/macrophages than classical M1 or M2 models (ref.18 and **Extended Data Fig.2**). Because flow cytometry antibodies were not available for any of the candidate genes, we used PrimeFlow to measure the dynamics of RNA transcription and found that expression of all 3 genes (*ETS2*, *BRWD1*, *PSMG1*) increased in unedited cells upon exposure to inflammatory stimuli (**Fig.1c**). Deletion of the chr21q22 enhancer did not affect the increase in *BRWD1* and *PSMG1* expression, but the upregulation of *ETS2* was significantly reduced (**Fig.1d**) – confirming that this pleiotropic locus functions as a distal *ETS2* enhancer in monocytes and monocyte-derived macrophages.

We next sought to discover the variant responsible for disease risk at the chr21q22 locus. Unfortunately, statistical fine-mapping – using the largest IBD GWAS to date[3] – could not identify the causal variant due to high linkage disequilibrium between the candidate single nucleotide polymorphisms (SNPs) (**Methods**, **Fig.1e**). We therefore used a high-throughput functional approach to first delineate the active enhancers at the locus, and then determine if any candidate SNPs within these regulatory regions might alter enhancer activity. This method – massively-parallel reporter assay (MPRA) – can simultaneously characterise enhancer activity in thousands of short DNA sequences by coupling each to a uniquely-barcoded reporter gene within an expression vector[19]. Genetic sequences that modulate gene expression can be identified by normalising the barcode counts in mRNA extracted from transfected cells to their equivalent counts in the input DNA library. After adapting the MPRA vector for use in primary macrophages (**Methods**, **Extended Data Fig.3**), we synthesised a pool of overlapping oligonucleotides (oligos) to tile the 2-kb region encompassing all candidate SNPs at chr21q22, and included additional oligos containing either risk or non-risk alleles for every variant. The resulting vector library was transfected into inflammatory macrophages from multiple donors – thus ensuring that a physiological repertoire of transcription factors would be present to interact with the chr21q22 genomic sequences. Using a sliding window analysis to map active enhancers across the tiling sequences, we identified a single 442-bp region of enhancer activity (chr21:40466236-

40466677, hg19; **Fig.1f**) that harboured three (of seven) candidate SNPs. Two of these polymorphisms were transcriptionally inert, but the third (rs2836882) had the strongest expression-modulating effect of any candidate variant, with the risk allele (G) significantly increasing transcription – consistent with the known eQTL (**Fig.1f**). Examining rs2836882 further, we noticed that this SNP lay within an experimentally-confirmed PU.1 ChIP-seq peak in human macrophages (**Fig.1g**). PU.1 is an important myeloid pioneer factor[20] that can bind to heterochromatin, initiate nucleosome remodelling – thus enabling other transcription factors to bind – and activate transcription[21]. To determine whether rs2836882 might affect PU.1 binding, we identified two publicly-available macrophage PU.1 ChIP-seq datasets from rs2836882 heterozygotes and used BaalChIP[22] to assess for allelic imbalances in PU.1 binding. Despite not lying within a canonical PU.1 binding motif, significant allele-specific PU.1 binding was detected at rs2836882, with over 4-fold greater binding to the risk allele in both datasets (**Fig.1h**). This result was replicated in TPP macrophages from five heterozygous donors by immunoprecipitating PU.1 and genotyping the bound DNA (**Extended Data Fig.4**). Together, this suggests that the rs2836882 risk allele should increase enhancer activity, consistent with the MPRA and eQTL results.

To test whether allele-specific enhancer activity was evident at the endogenous locus, we performed H3K27ac ChIP-seq in inflammatory macrophages from two rs2836882 major allele homozygotes and two minor allele homozygotes. While several nearby enhancer peaks were similar between these donors, the enhancer activity overlying rs2836882 was considerably stronger in major (risk) allele homozygotes (**Fig.1i**), contributing to a ~2.5-fold increase in enhancer activity across the extended chr21q22 locus (**Extended Data Fig.4**). Collectively, these data reveal a genetic mechanism whereby the putative causal variant at chr21q22 – identified via its functional consequences in primary macrophages – promotes binding of a pioneer transcription factor and increases the activity of a long-range *ETS2* enhancer.
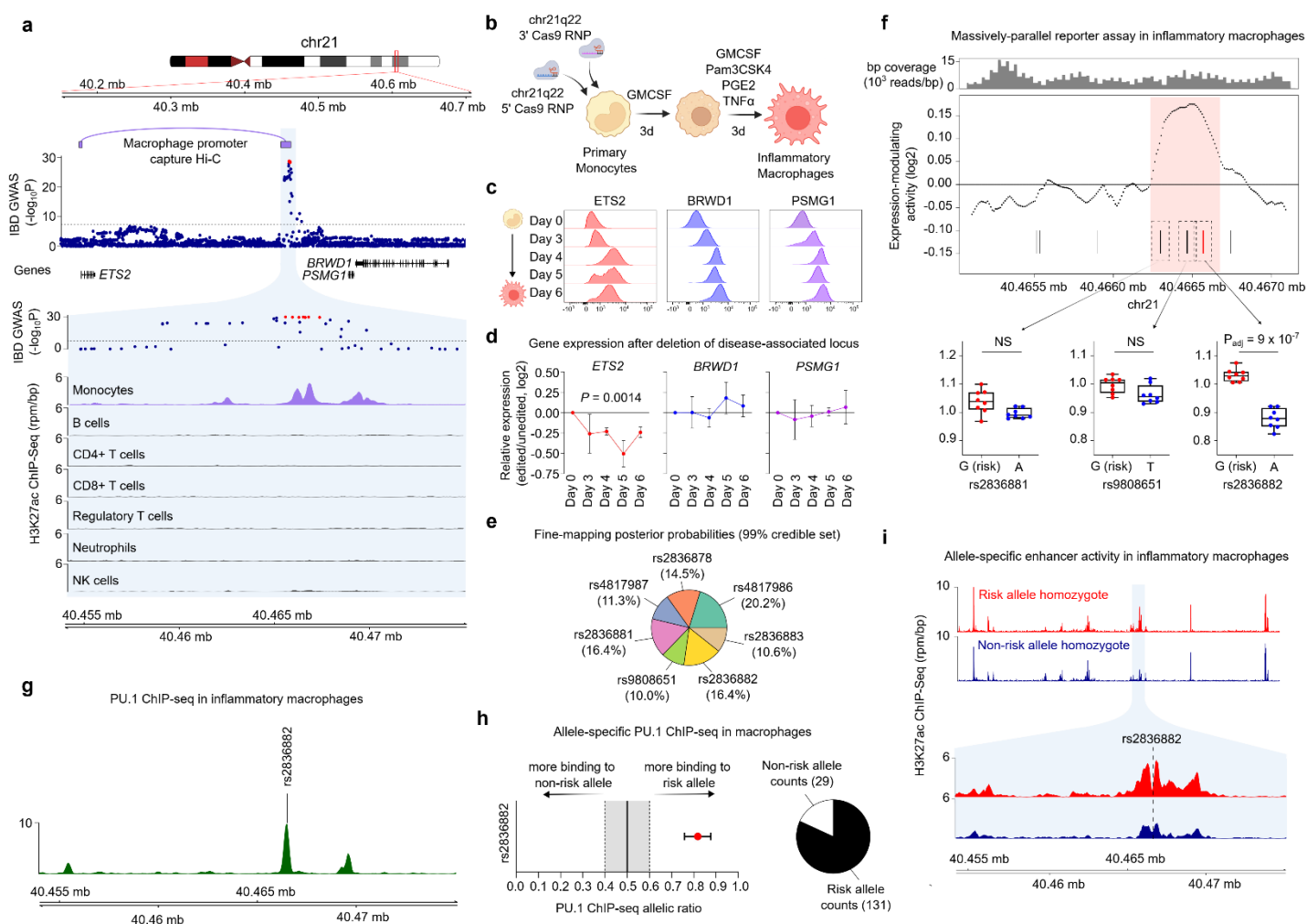
Figure 1. Resolving molecular mechanisms at chr21q22.

a. Annotation of the disease-associated chr21q22 locus depicting the IBD genetic association, physical interactions of the disease-associated haplotype in macrophages (promoter-capture Hi-C), and H3K27ac ChIP-seq data from various immune cell-types. **b.** Schematic of experiment to determine the function of the chr21q22 locus in monocyte-derived macrophages polarised under chronic inflammatory ("TPP") conditions. **c.** Histograms depicting the expression of *ETS2*, *BRWD1*, and *PSMG1* during inflammatory macrophage polarisation, measured using PrimeFlow RNA assays that quantify RNA by flow cytometry. Data are representative of one of four donors. **d.** Relative *ETS2*, *BRWD1*, and *PSMG1* expression in chr21q22-edited inflammatory macrophages (relative to non-targeting control cells; NTC). Plot shows log2 fold-change in mean fluorescence intensity (n=4, data represent mean±SEM, two-way ANOVA). **e.** SuSiE fine-mapping posterior probabilities for IBD-associated SNPs at the 21q22 locus (99% credible set). **f.** MPRA at the chr21q22 locus depicting oligonucleotide coverage (top), enhancer activity in inflammatory macrophages (analysed using a sliding window analysis of tiling oligos; middle), and expression-modulating effects of candidate SNPs within the identified enhancer (bottom) (n=8). Shaded region in enhancer activity plot indicates region of significant enhancer activity. **g.** PU.1 ChIP-seq peaks at the chr21q22 locus in macrophages. **h.** BaalChIP analysis of allele-specific PU.1 binding at rs2836882 in two heterozygous macrophage datasets (data represent 95% posterior distribution of allelic binding ratio) **i.** H3K27ac ChIP-seq data from major (top) or minor (bottom) allele homozygotes at the chr21q22 locus. Data are representative of two of four donors.

1   ETS2 is essential for macrophage inflammatory responses

2   Having identified a plausible mechanism by which the chr21q22 risk haplotype increases

3   *ETS2* expression, we sought to better understand the role of *ETS2* in

4   monocytes/macrophages. *ETS2* is a member of the ETS family of transcription factors, which

5   has been mainly studied as a proto-oncogene in cancer[23]. In contrast, the role of *ETS2* in

6   primary human macrophages has been less clearly defined, with previous studies using either

7   cell-lines or complex mouse models and largely focusing on a limited number of downstream

8   molecules[24-28]. This has led to contradictory reports, with *ETS2* being described as both

9   necessary and redundant for macrophage development[29,30], and both pro- and anti-

10   inflammatory[24-28]. To elucidate the specific role of *ETS2* in inflammatory human macrophages

11   – and determine how dysregulated *ETS2* expression might contribute to disease – we first

12   used a CRISPR-Cas9-based loss-of-function approach (**Fig.2a**). Two gRNAs targeting

13   different *ETS2* exons were designed, validated and individually incorporated into Cas9 RNPs

14   for transfection into primary monocytes – thereby minimising the chance that any effect was

15   due to off-target editing. These gRNAs resulted in on-target editing in ~89% and ~79% of total

16   cells respectively (**Extended Data Fig.2**). No differences in cell viability or expression of

17   macrophage markers were observed with either gRNA, suggesting that *ETS2* was not

18   required for inflammatory macrophage survival or differentiation (**Extended Data Fig.2**). In

19   contrast, production of pro-inflammatory cytokines, including IL-6, IL-8 and IL-1β, was

20   significantly reduced following *ETS2* disruption (**Fig.2b**), whereas IL-10 – an anti-inflammatory

21   cytokine – was less affected. TNFα secretion could not be assessed as it was included in the

22   differentiation culture. We therefore investigated whether *ETS2* was also required for other

23   macrophage effector functions. First, we examined phagocytosis using fluorescently-labelled

24   particles that can be detected by flow cytometry. Similar to pro-inflammatory cytokine

25   production, phagocytosis was significantly impaired following *ETS2* disruption (**Fig.2c**). We

26   next measured extracellular reactive oxygen species (ROS) production – a key effector

27   response that directly contributes to tissue damage in inflammatory disease[31]. Disrupting

28   *ETS2* profoundly reduced the oxidative burst following macrophage activation – an effect that

8

29   appeared to be due to reduced expression of key NADPH oxidase components (**Fig.2d**,

30   **Extended Data Fig.5**). Together, this suggests that *ETS2* is required for multiple effector

31   functions in inflammatory macrophages.

32   To better understand the molecular basis for these distinct functional effects, we performed

33   RNA-sequencing (RNA-seq) in *ETS2*-edited and unedited inflammatory macrophages from

34   multiple donors. Disruption of *ETS2* led to widespread transcriptional changes, with reduced

35   expression of many inflammatory genes, including several well-known initiators and amplifiers

36   of inflammation (**Fig.2e**). Affected gene classes included cytokines (e.g. *TNFSF10/TRAIL*,

37   *TNFSF13*, *IL1A, IL1B*), chemokines (e.g. *CXCL1*, *CXCL3*, *CXCL5*, *CCL2, CCL5*), secreted

38   effector molecules (e.g. *S100A8*, *S100A9*, *MMP14*, *MMP9*), cell surface receptors (e.g.

39   *FCGR2A*, *FCGR2C, TREM1*), pattern recognition receptors (e.g. *TLR2*, *TLR6*, *NOD2*), and

40   signalling molecules (e.g. *MAP2K*, *GPR84*, *NLRP3*). To better characterise the pathways

41   affected by *ETS2* deletion, we performed gene-set enrichment analysis (fGSEA) using the

42   Gene Ontology Biological Pathways dataset. This corroborated the observed functional effects

43   (**Fig.2f**), with the most negatively-enriched pathways (downregulated following *ETS2*

44   disruption) relating to macrophage activation, pro-inflammatory cytokine production,

45   phagocytosis and ROS production. Genes involved in macrophage migration were also

46   significantly downregulated, but gene sets relating to monocyte-to-macrophage differentiation

47   were not significantly affected – consistent with *ETS2* being required for inflammatory effector

48   functions, but not influencing monocyte-to-macrophage development. Although fewer genes

49   increased in expression following *ETS2* deletion (**Fig.2e**), positive enrichment was noted for

50   genes involved in aerobic respiration and oxidative phosphorylation (OXPHOS; **Fig.2f**) –

51   metabolic processes linked to anti-inflammatory macrophage behaviour[32]. Collectively, these

52   data identify an indispensable role for *ETS2* in a range of macrophage effector functions,

53   which could explain why dysregulated *ETS2* expression is associated with multiple

54   inflammatory diseases. Indeed, deletion of the disease-associated chr21q22 enhancer

55   phenocopied both the transcriptional and functional consequences of disrupting *ETS2* (**Fig.2g**,
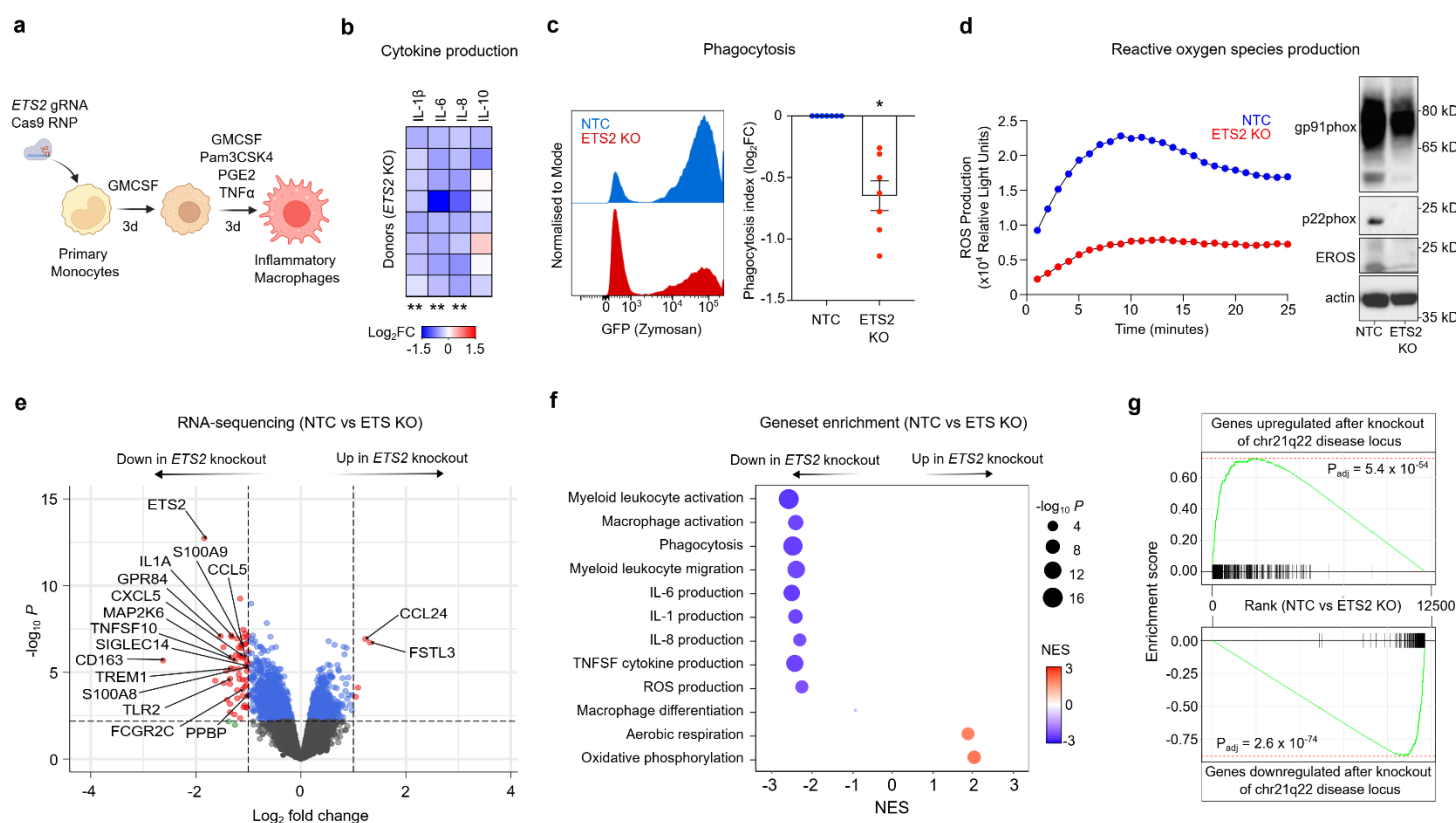
56   **Extended Data Fig.5**).

Figure 2. *ETS2* is essential for macrophage inflammatory responses.

a. Schematic of experiment for disrupting *ETS2* in primary monocytes and differentiating monocyte-derived macrophages under chronic inflammatory conditions. **b.** Macrophage cytokine secretion following *ETS2* disruption. Heatmap shows log2 fold-change of cytokine concentrations in the supernatants of *ETS2*-edited macrophages relative to unedited macrophages transfected with a non-targeting control gRNA-containing RNP (NTC). n=9, Wilcoxon matched-pairs test, two-tailed. **c.** Histogram depicting phagocytosis of fluorescently-labelled zymosan particles by *ETS2*-edited and unedited macrophages (left). Data representative of one of seven donors. Phagocytosis index in *ETS2*-edited and unedited macrophages (calculated as product of proportion and mean fluorescence intensity of phagocytosing cells; right). Plot depicts log2 fold-change in phagocytosis index for *ETS2*-edited macrophages relative to unedited cells (Wilcoxon signed-rank test, two-tailed; data represent mean±SEM). **d.** Production of ROS by *ETS2*-edited and unedited inflammatory macrophages (measured in relative light units; left). Data representative of one of six donors. Western blot for gp91*phox*, p22*phox*, and EROS expression in *ETS2*-edited and unedited macrophages (right). Data representative of one of three donors. **e.** Differentially-expressed genes in *ETS2*-edited versus unedited inflammatory macrophages (limma with voom transformation, n=8). **f.** Gene set enrichment analysis (fGSEA) of differentially-expressed genes between *ETS2*-edited and unedited inflammatory macrophages. Results of selected Gene Ontology Biological Pathways shown. Dot size represents *P*-value and colour denotes normalised enrichment score (NES). **g.** Enrichment of differentially-expressed genes following deletion of the disease-associated chr21q22 locus (upregulated genes, top; downregulated genes, bottom) in *ETS2*-edited versus unedited macrophages. * *P* < 0.05, ** *P* < 0.01.

10

ETS2 orchestrates macrophage inflammatory responses

57

58   Having found that *ETS2* was essential for monocyte-derived macrophage effector functions,

59   we next investigated whether it might also be sufficient to drive them – as would be expected

60   of a master regulator of inflammatory responses. This was particularly important because

61   although loss-of-function approaches can identify a gene's biological role(s), the chr21q22 risk

62   haplotype increases *ETS2* expression. To do this, we first optimised a method for controlled

63   overexpression of target genes in primary macrophages by transfecting defined amounts of *in*

64   *vitro* transcribed mRNA that was modified to minimise immunogenicity (**Fig.3a**, **Extended**

65   **Data Fig.3, Methods**). Resting, non-activated (M0) macrophages were then transfected with

66   mRNA encoding *ETS2* or its reverse complement – thereby controlling for quantity, length and

67   purine/pyrimidine composition of the transfected mRNA but with a transcript that would not be

68   translated (**Fig.3b**). After transfection, cells were exposed to low-dose lipopolysaccharide for 6

69   hours to initiate a low-grade inflammatory response that could be amplified if *ETS2* was

70   sufficient to drive inflammatory responses (**Fig.3a**). We first quantified secreted cytokines and

71   found that *ETS2* overexpression increased production of several pro-inflammatory cytokines,

72   although IL-10 was again less affected (**Fig.3c**). To better characterise the consequences of

73   *ETS2* overexpression, we performed RNA-seq and examined the macrophage activation

74   pathways that had required *ETS2*. Strikingly, all of these inflammatory pathways – including

75   macrophage activation, pro-inflammatory cytokine production, ROS production, phagocytosis

76   and migration – were induced in a dose-dependent manner following *ETS2* overexpression,

77   with greater enrichment of every pathway when more *ETS2* mRNA was transfected (**Fig.3d**).

78   This shows that *ETS2* is both necessary and sufficient for inflammatory responses in human

79   macrophages, consistent with being a master regulator of effector functions during chronic

80   inflammation, whose dysregulation is directly linked to human disease.

81

ETS2-regulated genes play a central role in IBD

82

83   To understand whether *ETS2* might contribute to the macrophage phenotype observed in

84   inflammatory disease, we compared the transcriptional consequences of overexpressing

85   *ETS2* with a gene signature of intestinal macrophages from Crohn's disease – one of the

86   conditions associated with the chr21q22 locus. Single cell RNA-seq analysis has previously

87   shown that active Crohn's disease is characterised by an expanded population of

88   inflammatory monocyte-derived macrophages that contributes to anti-TNFα resistance[7]. Using

89   the Crohn's disease macrophage signature as a gene set, we found that overexpressing

90   *ETS2* in resting macrophages induced a transcriptional state that closely resembled disease

91   macrophages, with core ("leading edge") enrichment of the majority of genes in the signature,

92   including many that encode therapeutic targets (**Fig.3e**).

93   Given the importance of *ETS2* in macrophage responses, and the fact that *ETS2*

94   overexpression phenocopied a disease-associated inflammatory state, we hypothesised that

95   other genetic associations might also implicate this previously uncharacterised pathway. An

96   important goal of GWAS was to identify key disease pathways[10], but this has proven

97   challenging due to a paucity of confidently-identified causal genes and a limited understanding

98   of how these are affected by genetic variation[10]. To better characterise the genetic risk

99   attributable to the macrophage ETS2 pathway, we focused on IBD since this has far more

100   genetic associations than any other chr21q22-associated disease. Examining the list of

101   commonly downregulated genes following *ETS2* editing (P_{adj} < 0.05 for both gRNAs), we

102   identified over 20 IBD risk genes – including many that have been proposed to be causal at

103   their respective loci[3,33] (**Extended Data Table 1**). These included genes that are thought to

104   affect macrophage biology (e.g. *SP140*, *LACC1/FAMIN*, *CCL2*, *CARD9*, *CXCL5, TLR4,*

105   *SLAMF8, FCGR2A*) as well as some that are highly expressed in macrophages but not

106   previously linked to specific pathways (e.g. *ADCY7*, *PTPRC*, *TAGAP*, *PTAFR*, *PDLIM5*). To

107   more formally assess the enrichment of an ETS2-regulated inflammatory pathway in IBD

108   genetics – and compare this to known disease pathways – we used SNPsea[34], an algorithm

109   designed to identify pathways affected by disease loci. 241 IBD-associated genetic loci were

110   tested for enrichment in 7,660 pathways, comprising 7,658 Gene Ontology Biological

12

111   Pathways and 2 overlapping lists of ETS2-regulated genes (either those downregulated

112   following *ETS2* editing or upregulated following *ETS2* overexpression). Significance of

113   enrichment was empirically computed using 5 million matched null SNP sets, and disease

114   pathways previously implicated by genetics were extracted for comparison. Strikingly, ETS2

115   target genes – however they were defined – were more strongly enriched for IBD-associated

116   loci than almost all previously implicated pathways, with not a single null SNP set showing

117   greater enrichment in either of the ETS2-regulated gene lists. After applying a stringent

118   Bonferroni multiple-testing correction, only ETS2-regulated genes and IBD pathways relating

119   to T cell activation, T-helper 17 cells, autophagy and IL-10 signalling showed significant

120   enrichment (**Fig.3f**). This suggests that ETS2 signalling in macrophages plays a fundamental

121   role in IBD pathogenesis, with stronger genetic enrichment than most previously implicated
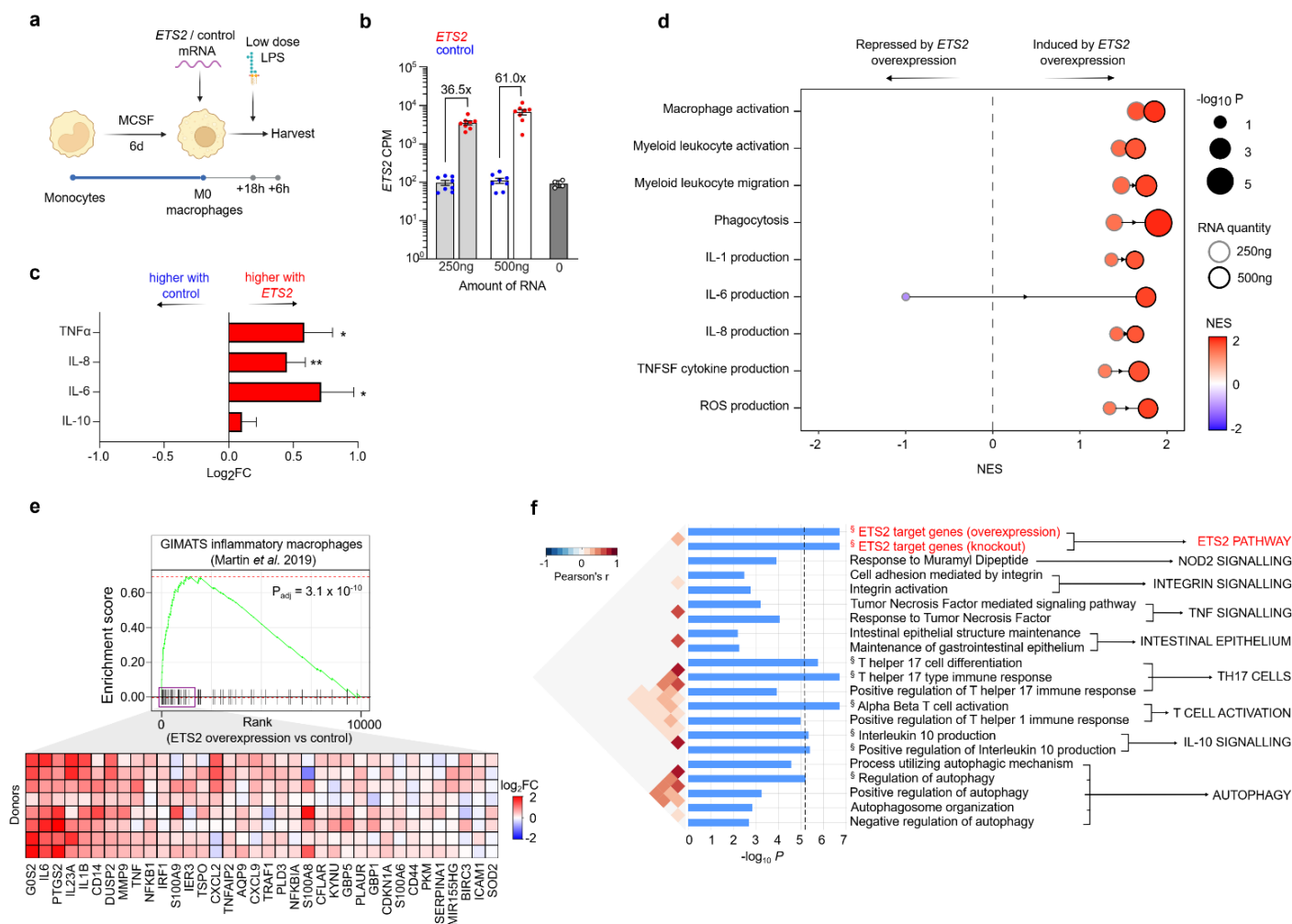
122   pathways.

13

Figure 3. ETS2 orchestrates macrophage inflammatory responses.

a. Schematic of *ETS2* overexpression experiment. Resting (M0) human macrophages were transfected with pre-defined amounts of *in vitro* transcribed *ETS2* mRNA or control mRNA (*ETS2* reverse complement), activated with low dose LPS (0.5ng/ml), and harvested. n=8. **b.** *ETS2* mRNA levels in macrophages transfected with *ETS2* or control mRNA or untransfected (from separate experiment). **c.** Cytokine secretion following *ETS2* overexpression. Plot shows log2 fold-change of cytokine concentrations in macrophage supernatants (*ETS2* relative to control) following transfection with 500ng mRNA. **d.** Gene set enrichment analysis (fGSEA) of differentially-expressed genes between *ETS2*-overexpressing and control macrophages. Results shown for the same Gene Ontology Biological Pathways that were negatively enriched following ETS2 editing. Dot size represents P-value, colour denotes normalised enrichment score (NES), and border colour denotes amount of transfected mRNA. **e.** Enrichment of a disease-associated inflammatory macrophage gene signature, derived from single cell RNA-seq of Crohn's disease intestinal biopsies, in *ETS2*-overexpressing macrophages (relative to control; top). Heatmap of leading-edge genes showing log2 fold-change of gene expression in *ETS2*-overexpressing macrophages relative to control (500ng mRNA; bottom). **f.** SNPsea analysis of enrichment of 241 IBD-associated loci within *ETS2*-regulated genes (red) and pathways previously linked to IBD pathogenesis (black). Significantly enriched pathways (Bonferroni-corrected permutation $P < 0.05$) indicated by §. * $P < 0.05$, ** $P < 0.01$.

ETS2 controls inflammatory responses via transcriptional and metabolic effects

We next sought to understand how *ETS2* controlled such diverse macrophage effector functions. Studying ETS2 biology is challenging because no ChIP-seq-grade antibodies exist, precluding direct identification of its transcriptional targets. Even the ENCODE project, which performed ChIP-seq for 181 transcription factors, was unable to directly immunoprecipitate ETS2[35]. We therefore first used a "guilt-by-association" approach to identify genes that were co-expressed with *ETS2* across 64 different human macrophage polarisation conditions[17]. This identified *PFKFB3* – encoding the rate-limiting enzyme of glycolysis – as the most highly co-expressed gene, with *HIF1A* also highly co-expressed (**Fig.4a**). Together, these genes are known to facilitate a "glycolytic switch" that is required for myeloid inflammatory responses[36]. We therefore hypothesised that *ETS2* might control inflammatory responses via metabolic reprogramming – a possibility supported by OXPHOS genes being negatively correlated with *ETS2* expression (**Fig.4a**) and upregulated following *ETS2* disruption (**Fig.2f**). To assess the metabolic consequences of disrupting *ETS2*, we quantified label incorporation from ^{13}C-glucose in edited and unedited inflammatory macrophages using gas chromatography–mass spectrometry (GC-MS). Widespread modest reductions in labelled and total glucose metabolites were detected following *ETS2* disruption (**Fig.4b, Extended Data Fig.6**). This affected both glycolytic and TCA cycle metabolites, with significant reductions in intracellular and secreted lactate, a hallmark of anaerobic glycolysis, and succinate, an important inflammatory signalling metabolite[37]. These results would be consistent with glycolytic suppression, with reductions in TCA metabolites being due to reduced flux into TCA and increased consumption by mitochondrial OXPHOS[38]. To determine whether metabolic changes were responsible for ETS2-mediated inflammatory effects, we treated *ETS2*-edited macrophages with roxadustat, a HIF1α stabiliser that promotes glycolysis via HIF1α-mediated metabolic reprogramming. This had the predicted effect on genes involved in glycolysis and OXPHOS, but did not rescue the effects of *ETS2* disruption, either transcriptionally or functionally (**Fig.4c, Extended Data Fig.6**). Thus, while disrupting *ETS2* does alter glycometabolism, this does not fully explain the observed differences in inflammation.

15

151   To try to elucidate the mechanism by which ETS2 controlled such diverse inflammatory

152   effects, we revisited whether we could directly identify ETS2 target genes. Using a range of

153   anti-ETS2 antibodies, we confirmed that none worked for ChIP-seq (data not shown) so

154   investigated whether any might work for Cleavage-Under-Targets-and-Release-Using-

155   Nuclease (CUT&RUN), which does not require formaldehyde fixation. One antibody identified

156   multiple, significantly-enriched genomic regions (peaks) of which 6,560 were reproducibly

157   detected across two biological replicates (Irreproducible Discovery Rate cut-off 0.01) with

158   acceptable quality metrics[39] (**Fig.4d**). These peaks were mostly located in active regulatory

159   regions (90% in promoters or active enhancers, **Fig.4e**) and were highly enriched for a

160   canonical ETS2 binding motif (4.02-fold enrichment over global controls, **Fig.4f**) – consistent

161   with being sites of ETS2 binding. After combining the biological replicates to improve peak

162   detection, we identified ETS2 binding at the promoters of many inflammatory genes, including

163   several that are essential for distinct macrophage functions, such as *NCF4* (encoding a key

164   NADPH oxidase component), *NLRP3* (encoding a key inflammasome component), and *TLR4*

165   (encoding a key pattern recognition receptor) (**Fig.4g**). Overall, 48.3% of genes dysregulated

166   following *ETS2* disruption, and 50.3% of genes dysregulated following *ETS2* overexpression,

167   contained an ETS2 binding peak within their core promoter or putative cis-regulatory elements

168   (**Fig.4h**) – consistent with ETS2 directly regulating a range of macrophage inflammatory

169   responses. Notably, these gene targets included *HIF1A*, *PFKFB3*, and other glycolytic genes

170   (e.g. *GPI*, *HK2*, and *HK3*), suggesting that the observed metabolic changes might be directly

171   induced by ETS2, rather than being solely attributable to differences in inflammation.

172   Intriguingly, we also detected ETS2 binding at its own enhancer at chr21q22 (**Fig.4i**). This is

173   consistent with reports that PU.1 and ETS2 can interact synergistically[40], and would implicate

174   a feed-forward mechanism at the disease-associated locus, where increased *ETS2*

175   expression reinforces *ETS2* enhancer activity. Together, these data implicate ETS2 as a

176   master regulator of monocyte/macrophage responses during chronic inflammation, capable of

177   directing a multifaceted effector programme, and creating a metabolic environment that is

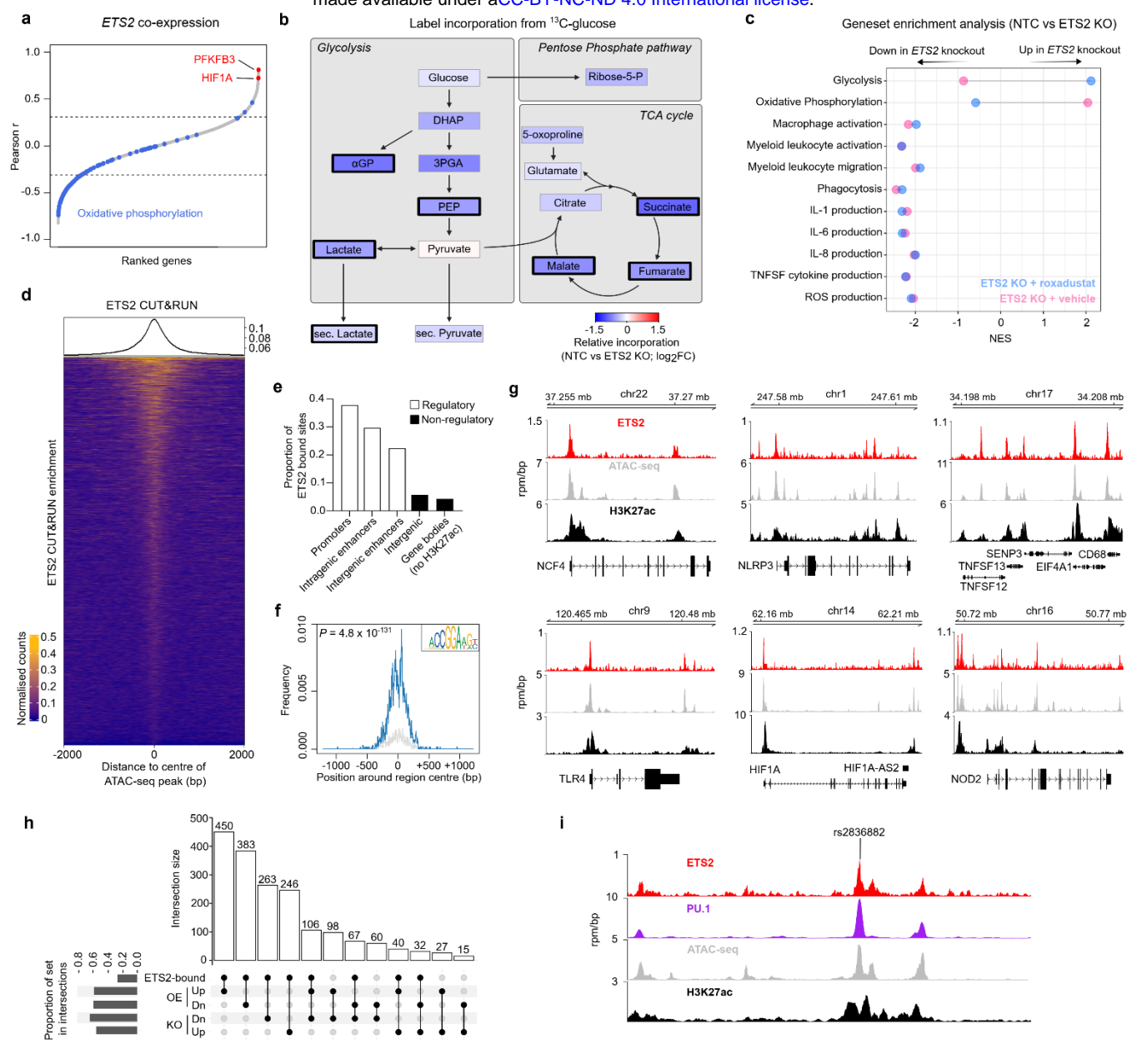178   permissive for inflammation.

16

Figure 4. ETS2 directs macrophage responses via transcriptional and metabolic effects.

a. Genes co-expressed with *ETS2* in 64 monocyte-derived macrophage datasets. Dotted lines equivalent to FDR $P < 0.05$. **b.** Effect of *ETS2* disruption on glucose metabolism. Colour denotes median log2 fold-change in label incorporation from ^{13}C-glucose in *ETS2*-edited cells relative to unedited cells. Bold black border denotes $P < 0.05$ (Wilcoxon matched-pairs, two-tailed, n=6). **c.** Gene set enrichment analysis (fGSEA) of differentially-expressed genes between *ETS2*-edited and unedited TPP macrophages, treated with either roxadustat or vehicle. Results for selected Gene Ontology Biological Pathways shown. **d.** Enrichment heatmap of *ETS2* CUT&RUN peaks (IDR cut-off 0.01, n=2) in accessible chromatin from TPP macrophages (4-kb regions centred on ATAC-seq peaks). **e.** Features of ETS2 binding sites (based on gene coordinates and H3K27ac ChIP-seq in TPP macrophages). **f.** Enrichment of an ETS2 binding motif in ETS2 CUT&RUN peaks (hypergeometric P-value). **g.** ETS2 binding, chromatin accessibility (ATAC-seq), and enhancer activity (H3K27ac) at selected loci. **h.** UpSet plot of intersections between ETS2 gene lists, including genes with ETS2 peaks in their core promoters or cis-regulatory elements and significantly up- (Up) or down-regulated (Dn) genes following ETS2 editing (KO) or overexpression (OE). Vertical bars denote shared genes between lists, indicated by connected dots in lower panel. Horizontal bars denote proportion of gene list within intersections. **i.** ETS2 binding, chromatin accessibility (ATAC-seq), and enhancer activity (H3K27ac) at the disease-associated chr21q22 locus.

17

179 **ETS2-driven inflammation is evident in diseased tissue and can be targeted**

180 **pharmacologically.**

181 The strong enrichment of IBD GWAS hits within ETS2-regulated genes led us to hypothesise

182 that the transcriptional footprint of this pathway might be generally detectable in the affected

183 tissues of chr21q22-associated diseases – a possibility that would have important therapeutic

184 implications. Using publicly-available gene expression data from diseases linked to chr21q22

185 – intestinal macrophages from IBD, synovium from ankylosing spondylitis (AS), and liver from

186 PSC – we confirmed that diseased tissue was significantly enriched for ETS2-regulated genes

187 (**Fig.5a, Extended Data Fig.7**). We therefore investigated whether this pathway could be

188 pharmacologically targeted. Specific ETS2 inhibitors do not exist and structural analyses

189 indicate that there is no allosteric inhibitory mechanism that could be easily targeted[41]. We

190 therefore used the NIH LINCS database to identify drugs that might modulate ETS2 activity[8].

191 This repository contains over 30,000 differentially-expressed genelists from cell-lines exposed

192 to over 6,000 small molecules. Using fGSEA, 906 drug signatures were found to mimic the

193 transcriptional effect of disrupting *ETS2* in inflammatory macrophages ($P_{adj} < 0.05$), including

194 several approved treatments for IBD and AS (e.g. JAK inhibitors). Of these candidate

195 therapies, the most common class were MEK inhibitors (**Fig.5b**), which are already licensed

196 for non-inflammatory human diseases (e.g. neurofibromatosis). This result was not due to a

197 single compound, but rather a class effect with multiple MEK1/2 inhibitors downregulating

198 ETS2 target genes (**Fig.5c**). This made biological sense, since MEK1 and MEK2 – together

199 with several other targets identified – are known upstream regulators of ETS-family

200 transcription factors (**Fig.5d**). Indeed, some of these drug classes, including MEK1/2 and

201 HSP90 inhibitors, have been reported to be beneficial in animal colitis models, although this is

202 often a poor indicator of clinical efficacy – with several approved IBD treatments being

203 ineffective in mice and many drugs that improve mouse models being ineffective in human

204 IBD[42]. To determine whether MEK inhibition would abrogate ETS2-driven inflammatory

205 responses in primary human macrophages, we differentiated monocytes under chronic

206 inflammatory conditions and treated them with a selective, non-ATP competitive MEK inhibitor

18

207 (PD-0325901; **Fig.5e**). We observed potent anti-inflammatory activity that phenocopied the

208 effect of disrupting *ETS2* or deleting the chr21q22 enhancer (**Fig.5f, Extended Data Fig.8**),

209 with downregulation of multiple ETS2-regulated pathways (including several drug targets;

210 **Fig.5g**). To further explore the therapeutic potential of targeting ETS2 signalling[42], we

211 employed a human gut explant model. Intestinal mucosal biopsies were obtained from

212 patients with active IBD, who were not receiving immunosuppressive or biologic therapies,

213 and cultured with either a MEK inhibitor or a negative or positive control (**Methods**). Release

214 of multiple IBD-associated inflammatory cytokines was significantly reduced by MEK inhibition

215 – to comparable levels observed with infliximab (an anti-TNFα antibody widely used for IBD;

216 **Fig.5h**). Moreover, we confirmed that expression of ETS2-regulated genes was reduced

217 (**Fig.5i, Extended Data Fig.8)** and that there was significant improvement in a validated

218 transcriptional inflammation score[43] that reflects IBD-associated inflammation and has been

219 shown to reduce upon effective therapy (**Fig.5j**). Together, this shows that targeting an

220 upstream regulator of *ETS2* can abrogate pathological inflammation in a chr21q22-associated

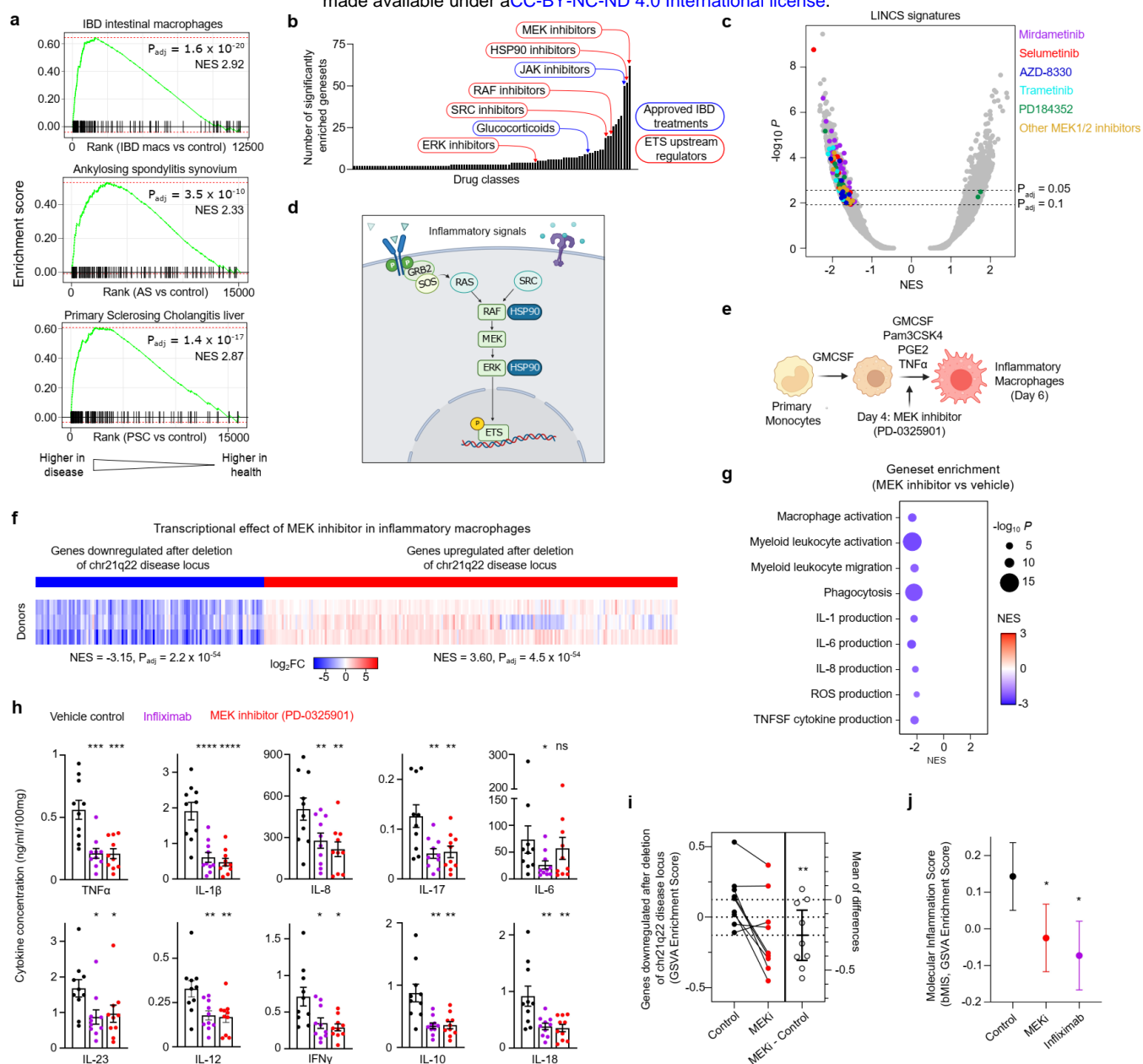221 disease, and may be useful therapeutically.

19

Figure 5. ETS2-driven inflammation is evident in disease and can be therapeutically targeted.

a. Enrichment of chr21q22-regulated genes in IBD intestinal macrophages (top), AS synovium (middle), and PSC liver (bottom). All relative to unaffected tissue. Gene set comprised significantly downregulated genes following chr21q22 deletion. **b.** Candidate drug classes (from NIH LINCS database) that phenocopy the transcriptional consequences of *ETS2* disruption. **c.** fGSEA results for NIH LINCS drug signatures (FDR *P* estimated using adaptive multi-level split Monte-Carlo scheme; NES, normalised enrichment score). Significantly enriched MEK inhibitor gene sets coloured by molecule. **d.** Schematic of known upstream regulators of *ETS*-family transcription factors. **e.** Schematic of experiment for treating inflammatory macrophages with a MEK inhibitor (PD-0325901) **f.** Heatmap of relative expression (log2 fold-change) of chr21q22-regulated genes in inflammatory macrophages following MEK inhibition (compared to vehicle control, n=3). **g.** fGSEA of differentially-expressed genes between MEK inhibitor-treated and control inflammatory macrophages. Results shown for Gene Ontology Biological Pathways that were negatively enriched following *ETS2* editing. Dot size represents *P*-value and colour denotes NES. **h.** Cytokine secretion from IBD mucosal biopsies cultured for 18 hours with vehicle control, PD-0325901, or infliximab. **i.** Estimation plot of GSVA enrichment scores for chr21q22-downregulated genes in IBD intestinal biopsies following MEK inhibition (MEKi). Error bars indicate 95%CI. **j.** GSVA enrichment scores of a biopsy-derived molecular inflammation score (bMIS). Data in **h** and **i** represent mean±SEM. Wilcoxon matched-pairs test, two-tailed, n=10 (h), n=9 (j). * *P* < 0.05, ** *P* < 0.01, *** *P* < 0.001, **** *P* < 0.0001.

Discussion

223   Arguably the greatest challenge in modern genetics is to translate the success of GWAS into a

224   better understanding of human disease. Here, we show how this can provide insights into

225   basic immunology as well as disease mechanisms, with investigation of a single pleiotropic

226   risk locus leading to the discovery of a master regulator of human macrophage responses and

227   a key pathogenic pathway that is potentially druggable. Monocyte-derived macrophages play

228   an important role in the pathogenesis of many inflammatory diseases[14], producing cytokines

229   that are often targeted therapeutically. Blocking individual cytokines, however, is typically only

230   effective in 30-40% of patients[44] and there is a growing realisation that modulating several

231   cytokines at once may be a better approach[45]. Modulating ETS2 signalling via MEK1/2

232   inhibition has a broad effect on multiple inflammatory cytokines, including TNFα, IL-23, and IL-

233   12 – all targets of existing therapies – and IL-1β which has previously been linked to

234   treatment-refractory IBD[46] but is not directly modulated by other small molecules (e.g. JAK

235   inhibitors). However, systemic use of MEK inhibitors may not be an ideal strategy for treating

236   chronic disease due to the physiological roles of MEK in other tissues. Indeed, use of MEK

237   inhibitors for other conditions is currently limited by severe opthalmic, cardiac, and pulmonary

238   toxicities[47]. Targeting ETS2 directly – for example using PROTACs or molecular glues – or

239   selectively delivering a MEK inhibitor to inflammatory macrophages via antibody-drug

240   conjugates could potentially overcome this toxicity, and provide a safer means of inhibiting

241   ETS2-driven inflammation.

242   These findings emphasise the importance of studying disease mechanisms beyond simple

243   changes in gene expression, especially since the overlap between the chr21q22 risk

244   haplotype and a macrophage eQTL had been noted previously[5] without any indication as to

245   the importance of the downstream biology. Indeed, it is even possible that *ETS2* is involved in

246   other human pathology, aside from diseases associated with the chr21q22 locus. For

247   example, Down's syndrome – caused by trisomy of chromosome 21 – was recently proposed

248   to be a cytokinopathy[48], with increased basal expression of multiple inflammatory cytokines,

249   including several that are specifically upregulated following *ETS2* overexpression (e.g. IL-1β,

250   TNFα, and IL-6). Whether the additional copy of the *ETS2* gene contributes to this phenotype

251   is unknown, but warrants further study. Relatedly, it is interesting to consider why a

252   polymorphism that increases susceptibility to multiple inflammatory diseases is so common

253   (risk allele frequency ~75% in Europeans and >90% in Africans, **Extended Data Fig.9**). One

254   possibility is that enhanced macrophage effector responses might provide a selective

255   advantage during infection, which would explain why the ancestral risk allele has not been

256   negatively selected. Recent studies have not found evidence for a strong selective sweep at

257   this locus within the past few thousand years[49,50], but more ancient selection – or balancing

258   selection maintaining variation – cannot be excluded, especially since rs2836882 appears to

259   be an exceptionally old SNP (conservatively estimated at >500,000 years old; **Extended Data**

260   **Fig.9**) and was even polymorphic between Neanderthals and Denisovans (**Extended Data**

261   **Fig.9**).

262   In summary, using an intergenic GWAS hit as a starting point, we have identified a druggable

263   pathway that is both necessary and sufficient for human macrophage responses during

264   chronic inflammation. Furthermore, we show how genetic dysregulation of this pathway – via

265   perturbation of pioneer factor binding at a critical long-range enhancer – confers susceptibility

266   to multiple inflammatory diseases. This highlights the considerable, yet largely untapped,

267   opportunity to better understand disease biology that is presented by non-coding genetic

268   associations.

References

269

270   1   Miller, F. W. The increasing prevalence of autoimmunity and autoimmune diseases: an
271   urgent call to action for improved understanding, diagnosis, treatment, and prevention.
272   *Curr Opin Immunol* **80**, 102266, doi:10.1016/j.coi.2022.102266 (2023).

273   2   Dowden, H. & Munro, J. Trends in clinical success rates and therapeutic focus. *Nat
274   Rev Drug Discov* **18**, 495-496, doi:10.1038/d41573-019-00074-z (2019).

275   3   de Lange, K. M. *et al.* Genome-wide association study implicates immune activation of
276   multiple integrin genes in inflammatory bowel disease. *Nat Genet* **49**, 256-261,
277   doi:10.1038/ng.3760 (2017).

278   4   International Genetics of Ankylosing Spondylitis, C. *et al.* Identification of multiple risk
279   variants for ankylosing spondylitis through high-density genotyping of immune-related
280   loci. *Nat Genet* **45**, 730-738, doi:10.1038/ng.2667 (2013).

281   5   Ji, S. G. *et al.* Genome-wide association study of primary sclerosing cholangitis
282   identifies new risk loci and quantifies the genetic relationship with inflammatory bowel
283   disease. *Nat Genet* **49**, 269-273, doi:10.1038/ng.3745 (2017).

284   6   Ortiz-Fernandez, L. *et al.* Identification of susceptibility loci for Takayasu arteritis
285   through a large multi-ancestral genome-wide association study. *Am J Hum Genet* **108**,
286   84-99, doi:10.1016/j.ajhg.2020.11.014 (2021).

287   7   Martin, J. C. *et al.* Single-Cell Analysis of Crohn's Disease Lesions Identifies a
288   Pathogenic Cellular Module Associated with Resistance to Anti-TNF Therapy. *Cell*
289   **178**, 1493-1508 e1420, doi:10.1016/j.cell.2019.08.008 (2019).

290   8   Stathias, V. *et al.* LINCS Data Portal 2.0: next generation access point for perturbation-
291   response signatures. *Nucleic Acids Res* **48**, D431-D439, doi:10.1093/nar/gkz1023
292   (2020).

293   9   Harrison, R. K. Phase II and phase III failures: 2013-2015. *Nat Rev Drug Discov* **15**,
294   817-818, doi:10.1038/nrd.2016.184 (2016).

295   10   Claussnitzer, M. *et al.* A brief history of human disease genetics. *Nature* **577**, 179-189,
296   doi:10.1038/s41586-019-1879-7 (2020).

297   11   King, E. A., Davis, J. W. & Degner, J. F. Are drug targets with genetic support twice as
298   likely to be approved? Revised estimates of the impact of genetic support for drug
299   mechanisms on the probability of drug approval. *PLoS Genet* **15**, e1008489,
300   doi:10.1371/journal.pgen.1008489 (2019).

301   12   Hnisz, D. *et al.* Super-enhancers in the control of cell identity and disease. *Cell* **155**,
302   934-947, doi:S0092-8674(13)01227-0 [pii]

303   10.1016/j.cell.2013.09.053 (2013).

304   13   Kugathasan, S. *et al.* Loci on 20q13 and 21q22 are associated with pediatric-onset
305   inflammatory bowel disease. *Nat Genet* **40**, 1211-1215, doi:10.1038/ng.203 (2008).

306   14   Park, M. D., Silvin, A., Ginhoux, F. & Merad, M. Macrophages in health and disease.
307   *Cell* **185**, 4259-4279, doi:10.1016/j.cell.2022.10.007 (2022).

308   15   Javierre, B. M. *et al.* Lineage-Specific Genome Architecture Links Enhancers and Non-
309   coding Disease Variants to Target Gene Promoters. *Cell* **167**, 1369-1384 e1319,
310   doi:10.1016/j.cell.2016.09.037 (2016).

311   16   Fairfax, B. P. *et al.* Innate immune activity conditions the effect of regulatory variants
312   upon monocyte gene expression. *Science* **343**, 1246949, doi:343/6175/1246949 [pii]

313   10.1126/science.1246949 (2014).

314   17   Xue, J. *et al.* Transcriptome-based network analysis reveals a spectrum model of
315   human macrophage activation. *Immunity* **40**, 274-288,
316   doi:10.1016/j.immuni.2014.01.006 (2014).

317   18   Kuo, D. *et al.* HBEGF(+) macrophages in rheumatoid arthritis induce fibroblast
318   invasiveness. *Sci Transl Med* **11**, doi:10.1126/scitranslmed.aau8587 (2019).

319   19   Melnikov, A. *et al.* Systematic dissection and optimization of inducible enhancers in
320   human cells using a massively parallel reporter assay. *Nat Biotechnol* **30**, 271-277,
321   doi:10.1038/nbt.2137 (2012).

322   20   Nerlov, C. & Graf, T. PU.1 induces myeloid lineage commitment in multipotent
323   hematopoietic progenitors. *Genes Dev* **12**, 2403-2412, doi:10.1101/gad.12.15.2403
324   (1998).

325   21   Heinz, S. *et al.* Simple combinations of lineage-determining transcription factors prime
326   cis-regulatory elements required for macrophage and B cell identities. *Mol Cell* **38**,
327   576-589, doi:10.1016/j.molcel.2010.05.004 (2010).

328   22   de Santiago, I. *et al.* BaalChIP: Bayesian analysis of allele-specific transcription factor
329   binding in cancer genomes. *Genome Biol* **18**, 39, doi:10.1186/s13059-017-1165-7
330   (2017).

331   23   Martinez, L. A. Mutant p53 and ETS2, a Tale of Reciprocity. *Front Oncol* **6**, 35,
332   doi:10.3389/fonc.2016.00035 (2016).

333   24   Wei, G. *et al.* Activated Ets2 is required for persistent inflammatory responses in the
334   motheaten viable model. *J Immunol* **173**, 1374-1379, doi:10.4049/jimmunol.173.2.1374
335   (2004).

336   25   Zhao, J., Huang, K., Peng, H. Z. & Feng, J. F. Protein C-ets-2 epigenetically
337   suppresses TLRs-induced interleukin 6 production in macrophages. *Biochem Biophys*
338   *Res Commun* **522**, 960-964, doi:10.1016/j.bbrc.2019.11.123 (2020).

339   26   Chung, S. W., Chen, Y. H. & Perrella, M. A. Role of Ets-2 in the regulation of heme
340   oxygenase-1 by endotoxin. *J Biol Chem* **280**, 4578-4584, doi:10.1074/jbc.M409125200
341   (2005).

342   27   Quinn, S. R. *et al.* The role of Ets2 transcription factor in the induction of microRNA-
343   155 (miR-155) by lipopolysaccharide and its targeting by interleukin-10. *J Biol Chem*
344   **289**, 4316-4325, doi:10.1074/jbc.M113.522730 (2014).

345   28   Ma, X. *et al.* Ets2 suppresses inflammatory cytokines through MAPK/NF-kappaB
346   signaling and directly binds to the IL-6 promoter in macrophages. *Aging (Albany NY)*
347   **11**, 10610-10625, doi:10.18632/aging.102480 (2019).

348   29   Aperlo, C., Pognonec, P., Stanley, E. R. & Boulukos, K. E. Constitutive c-ets2
349   expression in M1D+ myeloblast leukemic cells induces their differentiation to
350   macrophages. *Mol Cell Biol* **16**, 6851-6858, doi:10.1128/MCB.16.12.6851 (1996).

351   30   Henkel, G. W. *et al.* PU.1 but not ets-2 is essential for macrophage development from
352   embryonic stem cells. *Blood* **88**, 2917-2926 (1996).

353   31   Mittal, M., Siddiqui, M. R., Tran, K., Reddy, S. P. & Malik, A. B. Reactive oxygen
354   species in inflammation and tissue injury. *Antioxid Redox Signal* **20**, 1126-1167,
355   doi:10.1089/ars.2012.5149 (2014).

356   32   Kelly, B. & O'Neill, L. A. Metabolic reprogramming in macrophages and dendritic cells
357   in innate immunity. *Cell Res* **25**, 771-784, doi:10.1038/cr.2015.68 (2015).

33   Sazonovs, A. *et al.* Large-scale sequencing identifies multiple genes and rare variants associated with Crohn's disease susceptibility. *Nat Genet* **54**, 1275-1283, doi:10.1038/s41588-022-01156-2 (2022).

34   Slowikowski, K., Hu, X. & Raychaudhuri, S. SNPsea: an algorithm to identify cell types, tissues and pathways affected by risk loci. *Bioinformatics* **30**, 2496-2497, doi:10.1093/bioinformatics/btu326 (2014).

35   Dunham, I. *et al.* An integrated encyclopedia of DNA elements in the human genome. *Nature* **489**, 57-74, doi:nature11247 [pii]

10.1038/nature11247 (2012).

36   Cramer, T. *et al.* HIF-1alpha is essential for myeloid cell-mediated inflammation. *Cell* **112**, 645-657, doi:10.1016/s0092-8674(03)00154-5 (2003).

37   Tannahill, G. M. *et al.* Succinate is an inflammatory signal that induces IL-1beta through HIF-1alpha. *Nature* **496**, 238-242, doi:10.1038/nature11986 (2013).

38   Shiratori, R. *et al.* Glycolytic suppression dramatically changes the intracellular metabolic profile of multiple cancer cell lines in a mitochondrial metabolism-dependent manner. *Sci Rep* **9**, 18699, doi:10.1038/s41598-019-55296-3 (2019).

39   Landt, S. G. *et al.* ChIP-seq guidelines and practices of the ENCODE and modENCODE consortia. *Genome Res* **22**, 1813-1831, doi:10.1101/gr.136184.111 (2012).

40   Sevilla, L. *et al.* Bcl-XL expression correlates with primary macrophage differentiation, activation of functional competence, and survival and results from synergistic transcriptional activation by Ets2 and PU.1. *J Biol Chem* **276**, 17800-17807, doi:10.1074/jbc.M008270200 (2001).

41   Newman, J. A., Cooper, C. D., Aitkenhead, H. & Gileadi, O. Structural insights into the autoregulation and cooperativity of the human transcription factor Ets-2. *J Biol Chem* **290**, 8539-8549, doi:10.1074/jbc.M114.619270 (2015).

42   Koboziev, I., Karlsson, F., Zhang, S. & Grisham, M. B. Pharmacological intervention studies using mouse models of the inflammatory bowel diseases: translating preclinical data into new drug therapies. *Inflamm Bowel Dis* **17**, 1229-1245, doi:10.1002/ibd.21557 (2011).

43   Argmann, C. *et al.* Biopsy and blood-based molecular biomarker of inflammation in IBD. *Gut*, doi:10.1136/gutjnl-2021-326451 (2022).

44   Alsoud, D., Verstockt, B., Fiocchi, C. & Vermeire, S. Breaking the therapeutic ceiling in drug development in ulcerative colitis. *Lancet Gastroenterol Hepatol* **6**, 589-595, doi:10.1016/S2468-1253(21)00065-0 (2021).

45   Feagan, B. G. *et al.* Guselkumab plus golimumab combination therapy versus guselkumab or golimumab monotherapy in patients with ulcerative colitis (VEGA): a randomised, double-blind, controlled, phase 2, proof-of-concept trial. *Lancet Gastroenterol Hepatol* **8**, 307-320, doi:10.1016/S2468-1253(22)00427-7 (2023).

46   Friedrich, M. *et al.* IL-1-driven stromal-neutrophil interactions define a subset of patients with inflammatory bowel disease that does not respond to therapies. *Nat Med* **27**, 1970-1981, doi:10.1038/s41591-021-01520-5 (2021).

47   Klesse, L. J. *et al.* The Use of MEK Inhibitors in Neurofibromatosis Type 1-Associated Tumors and Management of Toxicities. *Oncologist* **25**, e1109-e1116, doi:10.1634/theoncologist.2020-0069 (2020).

403   48   Malle, L. *et al.* Autoimmunity in Down's syndrome via cytokines, CD4 T cells and
404   CD11c(+) B cells. *Nature* **615**, 305-314, doi:10.1038/s41586-023-05736-y (2023).

405   49   Irving-Pease, E. K. *et al.* The Selection Landscape and Genetic Legacy of Ancient
406   Eurasians. *bioRxiv*, 2022.2009.2022.509027, doi:10.1101/2022.09.22.509027 (2022).

407   50   Le, M. K. *et al.* 1,000 ancient genomes uncover 10,000 years of natural selection in
408   Europe. *bioRxiv*, 2022.2008.2024.505188, doi:10.1101/2022.08.24.505188 (2022).

409 **Methods**

410 **Analysis of existing data relating to chr21q22**

411 We used IBD GWAS summary statistics[3] to perform multiple causal variant fine-mapping

412 using susieR[51] with reference minor allele and LD information calculated from 503 European

413 samples from 1000 Genomes phase 3. All R analyses used v.4.2.1. Palindromic SNPs (A/T or

414 C/G) and any SNPs that didn't match by position or alleles were pruned before imputation

415 using the *ssimp* equations reimplemented in R. This did not affect any candidate SNP at

416 chr21q22. We obtained SuSiE fine mapping results for *ETS2* (with identifier

417 ENSG00000157557 or ILMN_1720158) in monocyte datasets from the eQTL Catalog.

418 Colocalisation analysis was performed using coloc v5.2.0[52] using a posterior probability of H4

419 (PP.H4.abf) > 0.5 to call colocalisation.

420 Raw H3K27ac ChIP-seq data from primary human immune cells were downloaded from Gene

421 Expression Omnibus (GEO series GSE18927 and GSE96014) and processed as described

422 previously[53].

423 Processed promoter-capture Hi-C data[15] from 17 primary immune cell-types were downloaded

424 from OSF (https://osf.io/u8tzp).

425

426 **Monocyte purification and macrophage differentiation**

427 Leukocyte cones from healthy donors were obtained from NHS Blood and Transplant

428 (Cambridge Blood Donor Centre, Colindale Blood Centre, or Tooting Blood Donor Centre).

429 Peripheral blood mononuclear cells (PBMCs) were isolated by density centrifugation

430 (Histopaque 1077, Sigma) and monocytes were positively selected using CD14 Microbeads

431 (Miltenyi Biotec). Macrophage differentiation was performed using conditions that model

432 chronic inflammation (TPP)[17]: 3 days GM-CSF (50ng/ml, Peprotech) followed by 3 days GM-

433 CSF, TNFα (50ng/ml, Peprotech), PGE$_2$ (1μg/ml, Sigma Aldrich), and Pam$_3$CSK4 (1μg/ml,

434 Invivogen). All cultures were performed at 37°C, 5% CO$_2$ in antibiotic-free RPMI1640 media

435 containing 10% FBS, GlutaMAX, and MEM Non-Essential Amino Acids (all ThermoFisher).

436 Cells were detached using Accutase (Biolegend).

27

437

Identifying a model of chronic inflammatory macrophages

Human monocyte-derived macrophage gene expression data files (n=299) relating to 64

different polarisation conditions were downloaded from Gene Expression Omnibus

(GSE47189) and quantile normalised. Data from biological replicates were summarised to the

median value for every gene. Gene set variation analysis[54] (using the *GSVA* package in R)

was performed to identify the polarisation condition that most closely resembled CD14+

monocytes/macrophages from active IBD – using disease-associated lists of differentially-

expressed[55].

CRISPR-Cas9 editing of primary human monocytes

gRNA sequences were designed using CRISPick (formerly GPP sgRNA Designer) and

synthesised by IDT. gRNA sequences: chr21q22 5' gRNA, CCUGGCUGCCUCGCGUUUCC;

chr21q22 3' gRNA, CCUCGUCCAACAGAGAGCAA; ETS2 gRNA1,

CAGACACAGAAUUACCCCAA; ETS2 gRNA2, UUGCUGCACGGGGUUAACAA. Alt-R

CRISPR-Cas9 Negative Control crRNA #1 (IDT) was used as a non-targeting control. Cas9-

gRNA ribonucleoproteins were assembled as described previously[53] and nucleofected into

$5x10^6$ monocytes in 100μL nucleofection buffer (Human Monocyte Nucleofection Kit, Lonza)

using a Nucleofector 2b (Lonza, program Y-001). After nucleofection, monocytes were

immediately transferred into 5ml of pre-warmed culture media in a 6-well flat-bottomed plate,

and differentiated into macrophages under TPP conditions. Editing efficiency was quantified

by PCR amplification of the target region in extracted DNA (chr21q22_Fw primer,

GGTGGGGAGAGTTCCAAAGG; chr21q22_Rv, TCACCCTTCACCTCTTTGCT;

ETS2_g1_Fw, TCCTGAAGGTCCCATGAAAG; ETS2_g1_Rv, TCATTATGGCTCTGGGGTTC;

ETS2_g2_Fw, GCGGCACATTCATATCACAC; ETS2_g2_Rv,

GCAGAATACCCCAAGCAAAA). Editing efficiency at the chr21q22 locus was measured via

quantification of amplified fragments (2100 Bioanalyzer, Agilent) as previously described[53].

464   Editing efficiency for individual gRNAs was assessed using the Inference of CRISPR Edits

465   tool[56] (ICE, Synthego).

466

467   **PrimeFlow RNA Assay**

468   RNA abundance was quantified by PrimeFlow (ThermoFisher) in chr21q22-edited and

469   unedited (NTC) cells on days 0, 3, 4, 5, and 6 of TPP differentiation. Target probes specific for

470   *ETS2* (Alexa Fluor 647), *BRWD1* (Alexa Fluor 568) and *PSMG1* (Alexa Fluor 568) were used

471   according to the manufacturer's instructions. Data were analysed using FlowJo v10 (BD

472   Biosciences).

473

474   **MPRA**

475   Overlapping oligonucleotides containing 114-nt of genomic sequence were designed to tile the

476   region containing chr21q22 candidate SNPs (99% credible set) at 50bp intervals. Six technical

477   replicates were designed for every genomic sequence, each tagged by a unique 11-nt

478   barcode. Additional oligonucleotides were included to test the expression-modulating effect of

479   every candidate SNP in the 99% credible set. Allelic constructs were designed as described

480   previously[53] and tagged by 30 unique 11-nt barcodes. Positive and negative controls were

481   included as described previously[53]. 170-nt oligonucleotides were synthesised as part of a

482   larger MPRA pool (Twist Biosciences) containing the 16-nt universal primer site

483   ACTGGCCGCTTCACTG, 114-nt variable genomic sequence, KpnI and XbaI restriction sites

484   (TGGACCTCTAGA), an 11-nt barcode, and the 17-nt universal primer site

485   AGATCGGAAGAGCGTCG. Cloning into the MPRA vector was performed as described

486   previously[53]. A suitable promoter for the MPRA vector (RSV) was identified by testing

487   promoter activities in TPP macrophages. The MPRA vector library was nucleofected into TPP

488   macrophages (5µg vector into $5x10^6$ cells) in 100µl nucleofection buffer (Human Macrophage

489   Nucleofection Kit, Lonza) using a Nucleofector 2b (program Y-011). To ensure adequate

490   barcode representation, a minimum of $2x10^7$ cells were nucleofected for every donor (n=8).

491   After 24 hours, RNA was extracted and sequencing libraries were made from mRNA or DNA

492   input vector as described previously[53]. Library pools (of 6 samples each) were sequenced on

493   an Illumina HiSeq2500 high output flow-cell (50bp, single-end reads) and data were pre-

494   processed as previously described[53]. To identify regions of enhancer activity, a paired t-test

495   was performed to identify genomic sequences that enhanced transcription. A sliding window

496   analysis (300-bp window) was then performed across all tiling sequences using the *les*

497   package in R. Expression-modulating variants were identified using QuASAR-MPRA[57], as

498   described previously[53].

499

500   **BaalChIP**

501   Publicly-available PU.1 ChIP-seq datasets from human macrophages were downloaded from

502   GEO, and BAM files were examined (using the IGV genome browser) to identify rs2836882

503   heterozygotes (i.e. files containing both A and G allele reads at chr21:40,466,570; hg19). Two

504   suitable samples were identified (GSM1681423 and GSM1681429) which were used for a

505   Bayesian analysis of allelic imbalances in PU.1 binding, with correction for biases introduced

506   by overdispersion and biases towards the reference allele – implemented in the *BaalChIP*

507   package[22] in R.

508

509   **Allele-specific PU.1 ChIP-genotyping**

510   A 100ml blood sample was taken from five healthy individuals who were heterozygous at

511   rs2836882 (assessed via Taqman genotyping, ThermoFisher). All participants provided written

512   informed consent. Ethical approval was provided by the London - Brent Regional Ethics

513   Committee (REC: 21/LO/0682). Monocytes were isolated from PBMC using CD14 Microbeads

514   (Miltenyi Biotec) and differentiated into inflammatory macrophages using TPP conditions[17].

515   Following differentiation, macrophages were detached using Accutase and cross-linked for 10

516   min in fresh media containing 1% formaldehyde. Cross-linking was quenched with glycine for

517   5 min (final concentration 0.125M). Nuclei preparation and shearing were performed as

518   described previously[53] with 10 cycles sonication (30s ON/30s OFF, Bioruptor Pico,

519   Diagenode). PU.1 was immunoprecipitated overnight at 4°C using a polyclonal anti-PU.1

520   antibody (1:25; Cell Signaling) with the SimpleChIP Plus kit (Cell Signaling). The ratio of

521   rs2836882 alleles in the PU.1-bound DNA was quantified in duplicate by TaqMan genotyping

522   (assay C___2601507_20). A standard curve was generated using fixed ratios of geneblocks

523   containing either the risk or non-risk allele (200-nt genomic sequence centred on rs2836882;

524   Genewiz).

525

526   **PU.1 MPRA-ChIP-seq**

527   The MPRA vector library was transfected into TPP macrophages from six healthy donors.

528   Assessment of PU.1 binding to SNP alleles was performed as described previously[53], with

529   minimal sonication (to remove contaminants while minimising chromatin shearing).

530   Immunoprecipitation was performed overnight at 4ºC using a polyclonal anti-PU.1 antibody

531   (1:25; Cell Signaling) with the SimpleChIP Plus kit (Cell Signaling). Sequencing libraries were

532   prepared from isolated plasmids as for MPRA and sequencing on a MiSeq (50bp, single-end

533   reads).

534

535   **H3K27ac ChIP-seq**

536   TPP macrophages from two rs2836882 major allele homozygotes and two minor allele

537   homozygotes were harvested, cross-linked, and quenched as described above. Donors were

538   identified through the NIHR BioResource. H3K27ac ChIP-seq was performed as described

539   previously[53] using an anti-H3K27ac antibody (1:250, Abcam) or an isotype control (1:500,

540   rabbit IgG, Abcam). Libraries were sequenced on a HiSeq4000 (50bp, single-end reads). Raw

541   data were processed, QC'd, and analysed as described previously[53] (see Code Availability).

542

543   **Assays of macrophage effector functions**

544   *Flow cytometry*

545   Expression of myeloid markers was assessed by flow cytometry (BD LSRFortessa™ X-20).

546   Panel: CD11b PE/Dazzle 594 (BioLegend), CD14 evolve605 (ThermoFisher), CD16 PerCP

547   (BioLegend), CD68 FITC (BioLegend), Live/Dead Fixable Aqua Dead Cell Stain

31

548   (ThermoFisher), and Fc Receptor Blocking Reagent (Miltenyi). Data were analysed using

549   FlowJo v10 (BD Biosciences).

550

551   *Cytokine quantification*

552   Supernatants were collected on day 6 of TPP macrophage culture and frozen. Cytokine

553   concentrations were quantified in duplicate via electrochemiluminescence using U-PLEX

554   assays (Meso Scale Diagnostics).

555

556   *Phagocytosis*

557   Phagocytosis was assessed using fluorescently-labelled Zymosan particles (Green Zymosan,

558   Abcam) according to the manufacturer's instructions. Cells were seeded at 10^5 cells/well in

559   96-well round bottom plates. Cytochalasin D (10μg/ml, ThermoFisher), an inhibitor of

560   cytoskeletal rearrangement, was used as a negative control. Phagocytosis was quantified via

561   flow cytometry, and a phagocytosis index was calculated (proportion of positive cells multiplied

562   by their mean fluorescence intensity).

563

564   *Extracellular ROS production*

565   Extracellular ROS production was quantified using a Diogenes Enhanced Superoxide

566   Detection Kit (National Diagnostics) according to the manufacturer's protocol. Cells were

567   seeded at a density of 10^5 cells/well and pre-stimulated with PMA (200ng/ml, Sigma Aldrich).

568

569   *Western blotting*

570   Western blotting was performed as described previously[58] using the following primary

571   antibodies: rabbit anti-gp91*phox*, rabbit anti-p22*phox* (both Santa Cruz), rabbit anti-

572   C17ORF62/EROS (Atlas), rabbit anti-actin (Abcam). Secondary antibody was anti-rabbit IgG-

573   horseradish peroxidase (Cell Signaling). Chemiluminescence was recorded on a ChemiDoc

574   Touch imager (Bio-Rad) following incubation of the membrane with ECL (ThermoFisher) or

575   SuperSignal West Pico PLUS (ThermoFisher) reagent.

32

576

RNA sequencing

578 RNA was isolated from macrophage lysates (AllPrep DNA/RNA Micro Kit, Qiagen) and

579 sequencing libraries prepared from 10ng RNA using the SMARTer Stranded Total RNA-Seq

580 Kit v2 - Pico Input Mammalian (Takara) following the manufacturer's instructions. Libraries

581 were sequenced on a NextSeq2000 (50bp, PE reads: CRISPR-based loss-of-function,

582 roxadustat and PD-0325901 experiments) or a NovaSeq6000 (100bp, PE reads:

583 overexpression experiments). Reads were trimmed using Trim Galore (Phred score 24),

584 filtered to remove reads < 20bp, and ribosomal reads were removed using the BBSplit

585 function of BBMap (BBMap, sourceforge.net/projects/bbmap/) with the Human ribosomal DNA

586 complete repeating unit (GenBank: U13369.1). Reads were aligned to the human genome

587 (hg38) using HISAT2 (ref.[59]) and converted to BAM files, sorted and indexed using

588 SAMtools[60]. Gene read counts were obtained with the featureCounts program[61] from

589 Rsubread using the GTF annotation file for human genome build GRCh38 (version 102).

590 Differential expression analysis was performed in R using the *limma* package[62] with the voom

591 transformation and including donor as a covariate.

592

Gene set enrichment analysis

594 GSEA was performed using the *fGSEA*[63] package in R. Gene sets were either obtained from

595 Gene Ontology Biological Pathways (downloaded from MSigDB), experimentally-derived

596 based on differential expression analysis, or sourced from published literature[7]. Pathways

597 shown in Figures 2-5 are: GO:0002274, GO:0042116, GO:0097529, GO:0006909,

598 GO:0071706, GO:0032732, GO:0032755, GO:0032757, GO:2000379, GO:0009060,

599 GO:0006119, and GO:0045649. Statistical significance was calculated using the adaptive

600 multilevel split Monte Carlo method.

601

***In vitro* transcription**

603 The cDNA sequence for *ETS2* (NM005329.5) preceded by a Kozak sequence was

604 synthesised and cloned into a TOPO vector. This was linearised and a PCR amplicon of the

605 *ETS2* gene generated, adding a T7 promoter and an AG initiation sequence (Phusion, NEB):

606 Fw primer: GCTAATACGACTCACTATAAGGACAGGCCACCATGAATGATTTCGGAATC, Rv

607 primer: TCAGTCCTCCGTGTCGG). A reverse complement (control) amplicon was also

608 generated: Fw primer:

609 GCTAATACGACTCACTATAAGGACAGGCCACCTCAGTCCTCCGTGTCGG, Rv primer:

610 GCCACCATGAATGATTTCGGAATC). These amplicons were used as templates for *in vitro*

611 transcription using the HiScribe T7 mRNA Kit with CleanCap® Reagent AG kit (NEB)

612 according to the manufacturer's instructions, but with substitution of N1-methyl-pseudouridine

613 for uridine and methylcytidine for cytidine (both Stratech) to minimise non-specific cellular

614 activation by the transfected mRNA. mRNA was purified using a MEGAclear Transcription

615 Clean-Up Kit (ThermoFisher) and polyadenylated using an E. coli Poly(A) Polymerase (NEB)

616 before further clean-up (MEGAclear), quantification and analysis of product size

617 (NorthernMax®-Gly gel, ThermoFisher). For optimising overexpression conditions, GFP

618 mRNA was produced using the same method: Fw primer

619 GCTAATACGACTCACTATAAGGACAGGCCACCATGGTGAGCAAGGGCGAG, Rv primer

620 TTACTTGTACAGCTCGTCCATGC).

621

622 **mRNA overexpression.**

623 Lipofectamine MessengerMAX (ThermoFisher) was diluted in Opti-MEM (1:75 v/v), vortexed

624 and incubated at room temperature for 10 minutes. IVT mRNA was then diluted in a fixed

625 volume of Opti-MEM (112.5µl per transfection), mixed with an equal volume of diluted

626 Lipofectamine MessengerMAX and incubated for a further 5 minutes at room temperature.

627 The transfection mix was then added dropwise to 2.5×10^6 M0 macrophages (pre-cultured for 6

628 days in a 6-well plate in antibiotic-free RPMI1640 macrophage media containing M-CSF

629 (50ng/ml, Peprotech) – with media change on d3). For GFP overexpression, cells were

630 detached using Accutase 18 hours after transfection and GFP expression was measured by

34

631   flow cytometry. For ETS2 / control overexpression, either 250ng or 500ng mRNA was

632   transfected and low dose LPS (0.5ng/ml) was added 18 hours after transfection, and cells

633   detached using Accutase 6 hours later (n=8 donors). Representative *ETS2* expression in

634   untransfected macrophages obtained from previous data (GSE193336).

635

636   **SNPsea**

637   Pathway analysis of 241 IBD-associated GWAS hits[3] was performed using SNPsea[34]. In brief,

638   linkage intervals were defined for every lead SNP based on the furthest correlated SNPs (r^2 >

639   0.5 in 1000 Genomes, EUR population) and extended to the nearest recombination hotspots

640   with recombination rate >3 cM/Mb. If no genes were present in this region, the linkage interval

641   was extended up- and down-stream by 500kb. Genes within linkage intervals were tested for

642   enrichment within 7,660 pathways, comprising 7,658 Gene Ontology Biological Pathways and

643   2 lists of ETS2-regulated genes (either those significantly downregulated following *ETS2*

644   disruption with gRNA1 or those significantly upregulated following ETS2 overexpression,

645   based on a consensus list obtained from differential expression analysis including all samples

646   and using donor and mRNA quantity as covariates). The analysis was performed using a

647   single score mode: assuming that only one gene per linkage interval is associated with the

648   pathway. A null distribution of scores for each pathway was performed by sampling random

649   SNP sets matched on the number of linked genes (5,000,000 iterations). A permutation *P*-

650   value was calculated by comparing the enrichment of the IBD-associated gene list with the

651   null distribution. Gene sets relating to the following IBD-associated pathways were extracted

652   for comparison: NOD2 signalling (GO:0032495), Integrin signalling (GO:0033627,

653   GO:0033622), TNFα signalling (GO:0033209, GO:0034612), Intestinal epithelium

654   (GO:0060729, GO:0030277), Th17 cells (GO:0072539, GO:0072538, GO:2000318), T cell

655   activation (GO:0046631, GO:0002827), IL-10 signalling (GO:0032613, GO:0032733), and

656   autophagy (GO:0061919, GO:0010506, GO:0010508, GO:1905037, GO:0010507).

657

658   **ETS2 co-expression**

659   Genes co-expressed with ETS2 across 64 human monocyte-derived macrophage polarisation

660   conditions (normalised data from GSE47189) were identified using the rcorr function in the

661   *Hmisc* package in R.

662

663   **^{13}C-glucose GC-MS**

664   *ETS2*-edited or unedited TPP macrophages were generated in triplicate for each donor and

665   on day 6, media was removed, cells washed with PBS, and new media with labelled glucose

666   was added. Labelled media: RPMI1640 Medium, no glucose (ThermoFisher); 10% FBS

667   (ThermoFisher); GlutaMAX (ThermoFisher); ^{13}C-labelled glucose (Cambridge Isotype

668   Laboratories). After 24 hours – a time point selected from a time-course to establish steady-

669   state conditions – supernatants were snap-frozen and macrophages detached by scraping.

670   Macrophages were washed three times with ice-cold PBS, counted, re-suspended in 600μl

671   ice-cold chloroform:methanol (2:1, v/v) and sonicated in a waterbath (3 x 8 mins). All

672   extraction steps were performed at 4°C as previously described[64]. Samples were analysed in

673   an Agilent 7890B-7000C GC–MS system. Spitless injection (injection temperature 270°C)

674   onto a DB-5MS (Agilent) was used, using helium as the carrier gas, in electron ionization

675   mode. The initial oven temperature was 70°C (2 min), followed by temperature gradients to

676   295 °C at 12.5 °C per min and to 320 °C at 25 °C per min (held for 3 min). Scan range was m/z

677   50-550. Data analysis was performed using in-house software MANIC (version 3.0), based on

678   the software package GAVIN[65]. Label incorporation was calculated by subtracting the natural

679   abundance of stable isotopes from the observed amounts. Total metabolite abundance was

680   normalised to the internal standard (scyllo-inositol[64]).

681

682   **Roxadustat**

683   *ETS2*-edited or unedited TPP macrophages were generated as described previously. On day

684   5 of culture, cells were detached (Accutase) and re-plated at a density of 10^5 cells/well in 96-

685   well round bottom plates in TPP media containing Roxadustat (FG-4592, 30μM). After 12

686   hours, cells were harvested for functional assays and RNA-seq as described.

687

CUT&RUN

689   Pre-cultured TPP macrophages were harvested and processed immediately using the

690   CUT&RUN Assay kit (Cell Signaling) according to the manufacturer's instructions but omitting

691   the use of ConA-coated beads. In brief, 5×10^5 cells per reaction were pelleted, washed, and

692   resuspended in Antibody Binding buffer. Cells were incubated with antibodies: anti-ETS2

693   (1:100, ThermoFisher) or IgG control (1:20, Cell Signaling) for 2h at 4°C. After washing in

694   Digitonin Buffer, cells were incubated with pA/G-MNase for 1h at 4°C. Cells were washed

695   twice in Digitonin Buffer, resuspended in the same buffer and cooled for 5 minutes on ice.

696   Calcium chloride was added to activate pA/G-MNase digestion (30 min, 4°C) before the

697   reaction was stopped and cells incubated at 37°C for 10 min to release cleaved chromatin

698   fragments. Supernatants were collected by centrifugation and DNA extracted using spin

699   columns (Cell Signaling). Library preparation was performed using a protocols.IO protocol

700   (dx.doi.org/10.17504/protocols.io.bagaibse) with the NEBNext Ultra II DNA Library Prep Kit.

701   Size selection was performed using AMPure XP beads (Beckman Coulter) and fragment sizes

702   assessed using an Agilent 2100 Bioanalyzer (High Sensitivity DNA kit). Equimolar pools of

703   indexed libraries were sequenced on a NovaSeq6000 (100bp PE reads). Raw data were

704   analysed using guidelines from the Henikoff lab[66]. Briefly, paired-end reads were trimmed

705   using Trim Galore and aligned to the human genome (GRCh37/hg19) using Bowtie2. BAM

706   files were sorted, merged (technical and, where indicated, biological replicates), re-sorted and

707   indexed using SAMtools. Picard was used to mark unmapped reads and SAMtools to remove

708   these reads, re-sort and re-index. Bigwig files were created using the deepTools

709   bamCoverage function. Processed data were initially analysed using the nf-core CUT&RUN

710   pipeline v3.0, using CPM normalisation and default MACS2 parameters for peak calling. This

711   analysis yielded acceptable quality metrics (including an average FRiP score of 0.23) but

712   there were a high number of peaks with low fold enrichment (<4) over control. We therefore

713   applied more stringent parameters for peak calling (--qvalue 0.05 -f BAMPE --keep-dup all -B -

714   -nomodel) and applied an irreproducible discovery rate (IDR; cut-off 0.001) to identify

715   consistent peaks between replicates – implemented in the *idr* package in R (code:

716   https://github.com/JamesLeeLab/chr21q22_manuscript/CUT&RUN/CUTRUN_pipeline.sh).

717   Enrichment of an ETS2 binding motif in consensus IDR peaks was calculated using

718   TFmotifView[67] using global genomic controls. Overlap between consensus IDR peaks and the

719   core promoter (-250bp to +35bp from TSS) and/or putative cis-regulatory elements of ETS2-

720   regulated genes was assessed using lists of differentially-expressed genes following *ETS2*

721   disruption with gRNA1 or *ETS2* overexpression (based on a consensus across mRNA doses,

722   as described earlier). Putative cis-regulatory elements were defined as shared interactions

723   (CHiCAGO score > 5) in monocyte, M0 and M1 macrophage samples from publicly-available

724   promoter-capture Hi-C data[15].

725

726   **ATAC-seq**

727   ATAC-seq in TPP macrophages was performed using the Omni-ATAC protocol[68] with the

728   following modifications: cell number was increased to 75,000 cells, cell lysis time was

729   increased to 5 minutes; volume of Tn5 transposase in the transposition mixture was doubled;

730   duration of the transposition step was extended to 40 minutes. Amplified libraries were

731   cleaned using AMPure XP beads (Beckman Coulter) and sequenced on a NovaSeq6000

732   (100bp PE reads). Data were processed as described previously[69].

733

734   **Chr21q22 disease datasets**

735   Publicly-available raw RNA-seq data from the affected tissues of chr21q22-associated

736   diseases (and controls from the same experiment) were downloaded from GEO: IBD

737   macrophages (GSE123141), primary sclerosing cholangitis liver (GSE159676), ankylosing

738   spondylitis synovium (GSE41038). Reads were trimmed, filtered, and aligned as described

739   earlier. For each disease dataset, a ranked list of genes was obtained by differential

740   expression analysis between cases and controls using *limma* with voom transformation. For

741   IBD macrophages, only IBD samples with active disease were included. fGSEA using ETS2-

742   regulated gene lists was performed as described.

38

743

LINCS signatures

745   31,027 lists of down-regulated genes following exposure of a cell line to a small molecule

746   were obtained from the NIH LINCS database[8] (downloaded in January 2021). These were

747   used as gene sets for fGSEA (as described) with a ranked list of genes obtained by differential

748   expression analysis between *ETS2*-edited and unedited TPP macrophages (gRNA1) – using

749   *limma* with voom transformation and donor as a covariate. Drug classes for gene sets with

750   FDR $P < 0.05$ were manually assigned based on known mechanisms of action.

751

PD-0325901

753   TPP macrophages were generated as described previously. On day 4 of culture, PD-0325901

754   (0.5μM, Sigma) or vehicle (DMSO) were added. Cells were harvested on day 6 and RNA was

755   extracted and sequenced as described.

756

Colonic biopsies

758   During colonoscopy, intestinal mucosal biopsies (6 per donor) were collected from 10 IBD

759   patients (7 ulcerative colitis, 3 Crohn's disease). All had endoscopically active disease and

760   were not receiving immunosuppressive or biologic therapies. All biopsies were collected from

761   a single inflamed site. All patients provided written informed consent. Ethical approval was

762   provided by the London - Brent Regional Ethics Committee (REC: 21/LO/0682). Biopsies were

763   collected into Opti-MEM and within 1 hour were weighed and placed in pairs onto a transwell

764   insert (ThermoFisher) – designed to create an air-liquid interface[70] – in a 24-well plate. Each

765   well contained 1ml media and was supplemented with either DMSO (vehicle control), PD-

766   0325901 (0.5μM) or infliximab (10μg/ml; MSD). Media: Opti-MEM I (Gibco); GlutaMAX

767   (ThermoFisher); 10% FBS (ThermoFisher); MEM Non-Essential Amino Acids (ThermoFisher);

768   1% sodium pyruvate (ThermoFisher); 1% penicillin/streptomycin (ThermoFisher); 50μg/ml

769   gentamicin (Merck). After 18 hours, supernatants and biopsies were snap frozen. Supernatant

770   cytokine concentrations were quantified using LEGENDplex Human Inflammation Panel

39

771 (Biolegend). RNA was extracted from biopsies and libraries prepared as described earlier

772 (n=9, RNA from one donor was too degraded). Sequencing was performed on a NovaSeq

773 6000 (100bp, PE reads). Data were processed as described earlier and GSVA was performed

774 for ETS2-regulated genes and biopsy-derived signatures of IBD-associated inflammation[43].

775

776 **Chr21q22 genotypes in archaic humans**

777 Using publicly available genomes from seven Neanderthal individuals[71-74], one Denisovan

778 individual[75], and one Neanderthal and Denisovan F1 individual[76], we called genotypes at the

779 disease-associated chr21q22 candidate SNPs from the respective BAM files using "bcftools

780 mpileup" with base and mapping quality options -q 20 -Q 20 -C 50 and using "bcftools call -m -

781 C alleles", specifying the two alleles expected at each site in a targets file (-T option). From the

782 resulting vcf file, we extracted the number of reads supporting the reference and alternative

783 alleles stored in the "DP4" field.

784

785 **Inference of Relate genealogy at rs2836882**

786 We used genome-wide genealogies previously inferred for samples of the Simons Genome

787 Diversity Project[77] dataset (https://reichdata.hms.harvard.edu/pub/datasets/sgdp/) using

788 Relate[78,79]. These genealogies were downloaded from

789 https://www.dropbox.com/sh/2gjyxe3kqzh932o/AAAQcipCHnySgEB873t9EQjNa?dl=0. Using

790 the inferred genealogies, the genealogy at rs2836882 (chr21:40466570) was plotted using the

791 TreeView module of Relate.

792

793 **Statistical methodology**

794 Statistical methods used in MPRA analysis, fGSEA, and SNPsea are described above. For

795 other analyses, comparison of continuous variables between paired samples in two groups

796 was performed using a Wilcoxon matched-pairs test for non-parametric data or a paired t-test

797 for parametric data. Comparison against a hypothetical value was performed using a Wilcoxon

798 signed-rank test for non-parametric data or one sample t-test for parametric data. A Shapiro-

799   Wilk test was used to confirm normality. Two-tailed tests were used as standard unless a

800   specific hypothesis was being tested. Sample sizes are provided in respective sections.

801

802   **Code availability**

803   Code to reproduce analyses are available at

804   https://github.com/JamesLeeLab/chr21q22_manuscript and

805   https://github.com/chr1swallace/ibd-ets2-analysis.

806

807   **Data availability**

808   The datasets produced in this study, including raw and processed files, have been uploaded

809   to the following databases and will be made publicly available in advance of publication.

810   Gene Expression Omnibus: MPRA (GSE229472), RNA-seq of *ETS2* or chr21q22-edited TPP

811   macrophages (GSE229569), RNA-seq of *ETS2* overexpression (GSE229744), RNA-seq of

812   MEK inhibitor-treated TPP macrophages (GSE229743), H3K27ac ChIP-seq in TPP

813   macrophages (GSE229464), ATAC-seq in TPP macrophages (GSE229624), ETS2

814   CUT&RUN (GSE229745), biopsy RNA-seq data (GSE230020).

815   MetaboLights: Metabolomics (MTBLS7665).

Methods references

51   Zou, Y., Carbonetto, P., Wang, G. & Stephens, M. Fine-mapping from summary data with the "Sum of Single Effects" model. *PLoS Genet* **18**, e1010299, doi:10.1371/journal.pgen.1010299 (2022).

52   Wallace, C. A more accurate method for colocalisation analysis allowing for multiple causal variants. *PLoS Genet* **17**, e1009440, doi:10.1371/journal.pgen.1009440 (2021).

53   Bourges, C. *et al.* Resolving mechanisms of immune-mediated disease in primary CD4 T cells. *EMBO Mol Med* **12**, e12112, doi:10.15252/emmm.202012112 (2020).

54   Hanzelmann, S., Castelo, R. & Guinney, J. GSVA: gene set variation analysis for microarray and RNA-seq data. *BMC Bioinformatics* **14**, 7, doi:10.1186/1471-2105-14-7 (2013).

55   Peters, J. E. *et al.* Insight into Genotype-Phenotype Associations through eQTL Mapping in Multiple Cell Types in Health and Immune-Mediated Disease. *PLoS Genet* **12**, e1005908, doi:10.1371/journal.pgen.1005908 (2016).

56   Conant, D. *et al.* Inference of CRISPR Edits from Sanger Trace Data. *CRISPR J* **5**, 123-130, doi:10.1089/crispr.2021.0113 (2022).

57   Kalita, C. A. *et al.* QuASAR-MPRA: accurate allele-specific analysis for massively parallel reporter assays. *Bioinformatics* **34**, 787-794, doi:10.1093/bioinformatics/btx598 (2018).

58   Randzavola, L. O. *et al.* EROS is a selective chaperone regulating the phagocyte NADPH oxidase and purinergic signalling. *Elife* **11**, doi:10.7554/eLife.76387 (2022).

59   Kim, D., Paggi, J. M., Park, C., Bennett, C. & Salzberg, S. L. Graph-based genome alignment and genotyping with HISAT2 and HISAT-genotype. *Nat Biotechnol* **37**, 907-915, doi:10.1038/s41587-019-0201-4 (2019).

60   Li, H. *et al.* The Sequence Alignment/Map format and SAMtools. *Bioinformatics* **25**, 2078-2079, doi:10.1093/bioinformatics/btp352 (2009).

61   Liao, Y., Smyth, G. K. & Shi, W. featureCounts: an efficient general purpose program for assigning sequence reads to genomic features. *Bioinformatics* **30**, 923-930, doi:10.1093/bioinformatics/btt656 (2014).

62   Ritchie, M. E. *et al.* limma powers differential expression analyses for RNA-sequencing and microarray studies. *Nucleic Acids Res* **43**, e47, doi:10.1093/nar/gkv007 (2015).

63   Korotkevich, G. *et al.* Fast gene set enrichment analysis. *bioRxiv*, 060012, doi:10.1101/060012 (2021).

64   Bussi, C. *et al.* Lysosomal damage drives mitochondrial proteome remodelling and reprograms macrophage immunometabolism. *Nat Commun* **13**, 7338, doi:10.1038/s41467-022-34632-8 (2022).

65   Behrends, V., Tredwell, G. D. & Bundy, J. G. A software complement to AMDIS for processing GC-MS metabolomic data. *Anal Biochem* **415**, 206-208, doi:10.1016/j.ab.2011.04.009 (2011).

66   Meers, M. P., Bryson, T. D., Henikoff, J. G. & Henikoff, S. Improved CUT&RUN chromatin profiling tools. *Elife* **8**, doi:10.7554/eLife.46314 (2019).

67   Leporcq, C. *et al.* TFmotifView: a webserver for the visualization of transcription factor motifs in genomic regions. *Nucleic Acids Res* **48**, W208-W217, doi:10.1093/nar/gkaa252 (2020).

68   Corces, M. R. *et al.* An improved ATAC-seq protocol reduces background and enables interrogation of frozen tissues. *Nat Methods* **14**, 959-962, doi:10.1038/nmeth.4396 (2017).

69   Calderon, D. *et al.* Landscape of stimulation-responsive chromatin across diverse human immune cells. *Nat Genet* **51**, 1494-1505, doi:10.1038/s41588-019-0505-9 (2019).

70   Vadstrup, K. *et al.* Validation and Optimization of an Ex Vivo Assay of Intestinal Mucosal Biopsies in Crohn's Disease: Reflects Inflammation and Drug Effects. *PLoS One* **11**, e0155335, doi:10.1371/journal.pone.0155335 (2016).

71   Prufer, K. *et al.* The complete genome sequence of a Neanderthal from the Altai Mountains. *Nature* **505**, 43-49, doi:10.1038/nature12886 (2014).

72   Prufer, K. *et al.* A high-coverage Neandertal genome from Vindija Cave in Croatia. *Science* **358**, 655-658, doi:10.1126/science.aao1887 (2017).

73   Hajdinjak, M. *et al.* Reconstructing the genetic history of late Neanderthals. *Nature* **555**, 652-656, doi:10.1038/nature26151 (2018).

74   Mafessoni, F. *et al.* A high-coverage Neandertal genome from Chagyrskaya Cave. *Proc Natl Acad Sci U S A* **117**, 15132-15136, doi:10.1073/pnas.2004944117 (2020).

75   Meyer, M. *et al.* A high-coverage genome sequence from an archaic Denisovan individual. *Science* **338**, 222-226, doi:10.1126/science.1224344 (2012).

76   Slon, V. *et al.* The genome of the offspring of a Neanderthal mother and a Denisovan father. *Nature* **561**, 113-116, doi:10.1038/s41586-018-0455-x (2018).

77   Mallick, S. *et al.* The Simons Genome Diversity Project: 300 genomes from 142 diverse populations. *Nature* **538**, 201-206, doi:10.1038/nature18964 (2016).

78   Speidel, L., Forest, M., Shi, S. & Myers, S. R. A method for genome-wide genealogy estimation for thousands of samples. *Nat Genet* **51**, 1321-1329, doi:10.1038/s41588-019-0484-x (2019).

79   Speidel, L. *et al.* Inferring Population Histories for Ancient Genomes Using Genome-Wide Genealogies. *Mol Biol Evol* **38**, 3497-3511, doi:10.1093/molbev/msab174 (2021).

Acknowledgements

Author contributions

Conceptualisation, J.I.M., P.S., M.Z.C., C.W., D.C.T., J.C.L.; Methodology, C.T.S., C.B., M.S.D.S., L.O.R., L.S., J.I.M., C.W., J.C.L.; Software, C.B., M.S.D.S., L.S., J.I.M., C.W.;

44

916   Investigation, C.T.S., C.B., T.T.S., A.P.P., C.P.J., I.P., M.S.D.S., L.O.R., L.S., E.C.P., W.E.,

917   A.P.R., C.D.M., C.W, J.C.L.; Resources, C.T.S., C.B., M.S.D.S., J.C.L.; Formal analysis,

918   C.T.S., C.B., M.S.D.S., L.S., C.W., J.C.L.; Writing – Original Draft, C.T.S., C.B., J.C.L.; Writing

919   – Review & Editing, all authors; Funding Acquisition, J.C.L.; Supervision, J.I.M., P.S., C.W.,

920   D.C.T., J.C.L.

921

922   **Competing Interests**

923   C.T.S., C.B. and J.C.L. are co-inventors on a patent application relating to this work. C.W.

924   holds a part time position at GSK. GSK had no role in this study.

925

926   **Additional information**

927   **Supplementary information:** results of differential expression analysis in *ETS2*-edited or

928   *ETS2* overexpression experiments are available in Supplementary Tables 1 and 2.

929   **Correspondence and requests for materials** should be addressed to James C. Lee.